LA-UR-16-25422 (Accepted Manuscript)

TLR7 agonists induce transient viremia and reduce the viral reservoir in SIV-infected rhesus macaques on antiretroviral therapy

Lim, So-Yon; Hraber, Peter Thomas; Hesselgesser, Joe; Osuna, Christa E.; Gerold, Jefferey M; Hill, Allison L.; Barnes, Tiffany L.; Sanisetty, Srisowmya; Seaman, Michael S.; Lewis, Mark G.; Miller, Michael; Cihlar, Tomas; Lee, William; Gelezunias, Romas; Whitney, James B.

To be published in: Science Translational Medicine

DOI to publisher's version: 10.1126/scitranslmed.aao4521

Permalink to record: http://permalink.lanl.gov/object/view?what=info:lanl-repo/lareport/LA-UR-16-25422

TLR7 Agonists Induce Transient Viremia and Reduce the Viral Reservoir in SIV-Infected Monkeys on Antiretroviral Therapy

So-Yon Lim[1], Christa E. Osuna[1], Joe Hesselgesser[2], Peter T. Hraber[3] Jeffrey M. Gerold[4], Tiffany L. Barnes[2], Srisowmya Sanisetty[1], Michael S. Seaman[1], Mark G. Lewis[5], Romas Gelezunias[2], Michael D. Miller[2], Tomas Cihlar[2], William A. Lee[2], Alison L. Hill[4] and James B. Whitney[1,6*]

[1]Center for Virology and Vaccine Research, Beth Israel Deaconess Medical Center, Harvard Medical School, Boston, MA 02215, USA; [2]Gilead Sciences Inc., Foster City, CA 94404; [3]Los Alamos National Laboratory, Los Alamos, NM 87545; [4]Program for Evolutionary Dynamics, Harvard University, Cambridge, MA 02138 USA; [5]Bioqual, Rockville, MD 20852, USA; [6]Ragon Institute of MGH, MIT, and Harvard, Cambridge, MA 02139, USA

*Corresponding author

Abstract

Antiretroviral therapy can halt HIV-1 replication, but fails to target the long-lived latent viral reservoir. Several pharmacological compounds have been evaluated for their ability to reverse HIV-1 latency, but none have demonstrably reduced the latent HIV-1 reservoir, or impacted viral rebound following the interruption of antiretroviral therapy. Here, we evaluate orally administered selective toll-like receptor 7 agonists GS-986 and GS-9620 for their ability to induce transient viremia in simian immunodeficiency virus-infected rhesus monkeys on suppressive antiretroviral therapy. In an initial dose-escalation study, and a subsequent dose-optimization study, we found that toll-like receptor 7 agonists activate multiple innate and adaptive immune cell populations in addition to inducing SIV RNA. We also observed toll-like receptor 7 agonist–induced reductions in SIV DNA and *ex vivo* inducible virus from treated animals. In a second study, after stopping antiretroviral therapy, two of nine treated animals have remained aviremic for more than two years, even after *in vivo* CD8+ lymphocyte depletion. Moreover, adoptive transfer of cells from aviremic animals could not induce *de novo* infection in naïve recipient macaques. These findings suggest that toll-like receptor agonists may facilitate reservoir reduction in a subset of individuals.

Introduction

The HIV-1 latent reservoir persists despite long-term antiretroviral therapy (ART)(*1, 2*), necessitating the development of novel strategies for viral eradication(*3, 4*). Latency reversal agents (LRAs) have been evaluated as a potential means to reduce the HIV-1 reservoir (*4, 5*). Early clinical studies of LRAs have provided evidence of modest HIV-1 activation(*6-9*), but have failed to reduce the viral reservoir(*9-14*). First generation LRAs, such as histone deacetylase (HDAC) inhibitors, may also harbor immunosuppressive properties that may not be compatible with some therapeutic strategies aimed at HIV-1 eradication(*15, 16*). Collectively, these studies underscore the need for the continued development of novel, safe, and efficacious LRAs.

We sought to evaluate potent, selective, and orally-delivered small-molecule agonists of toll-like receptor 7 (TLR7) that induce potent immune responses and thus may impact the HIV-1 reservoir. GS-9620 is a TLR7 agonist that has demonstrated antiviral activity in animal models of hepatitis B virus that has already progressed to advanced clinical testing(*17-19*). The GS-9620 analog, GS-986, has been used as an investigational tool compound and possesses a similar pharmacological profile to GS-9620.

Results

To assess the therapeutic potential of TLR7 agonists *in vivo,* we selected twenty-one Indian origin rhesus monkeys (RMs) that did not express the MHC class I alleles *Mamu*-A*01, -B*08, or -B*17, which are associated with enhanced control of SIV RNA(*20*). All RMs were infected intrarectally (IR) with SIVmac251 using a repeat low-dose mucosal challenge protocol as described(*21*). Once infection was confirmed, all animals began a highly potent ART regimen of tenofovir (TFV), emtricitabine (FTC) and dolutegravir (DTG) as a daily subcutaneous injection at day 65 post-infection, as described(*22*). Plasma SIV RNA was assessed longitudinally throughout the study. On ART, plasma SIV RNA in all RMs declined rapidly and remained undetectable (SIV RNA at < 50 copies/mL blood) (**figure S1A**). After approximately 400 days of ART suppression, animals were divided into two study cohorts, and then into separate treatment and control arms for each study (**figure S2**).

At study assignment, prior to the initiation of TLR7 agonist dosing, there were no significant differences in the area-under-the-curve (AUC) viral burden (range, log 8.0-9.3), median plasma SIV pre-ART (range, log 4.5-6.6 RNA copies/ml), time to viral suppression (range, 14-103 days), or CD4+ and CD8+ T cell indices (CD4+, 256-1486 vs. 557-1316; CD8+, 552-1048 vs. 309-1283, respectively) between groups (**figure S1B**).

Our first study (Study 1) used 10 SIV-infected RMs that had been on ART for more than 437 days prior to TLR7 agonist dosing. GS-986 was dose-escalated in 4 of 10 RMs with administration every other week (EOW) by oral gavage, while the remaining 6 RMs served as controls. The initial dose of GS-986 was 0.1 mg/kg followed by a dose at 0.2mg/kg and then five doses at 0.3 mg/kg (**figure S2A**).

We longitudinally monitored several immunologic and virologic parameters prior to, during, and after GS-986 dosing. The activation of major lymphocyte subsets in the peripheral blood following each dose of GS-986 was measured by surface expression of CD69. All cell types evaluated (CD4+ T, CD8+ T, B and NK cells) were transiently activated within 24-48 hours post GS-986 treatment and returned to baseline prior to the next dose (**Fig. 1A**). However, CD8+ T and NK cells showed the greatest change in percentage activation after GS-986 administration. With the exception of B cells, cellular activation was dose dependent and plateaued during repeated dosing at 0.3 mg/kg (doses 4-7). The average increase in percentage of CD4+ T-cell activation following GS-986 treatment was 1-2% of the population, whereas 20-25% of NK and CD8+ T cells became activated. As expected, for the selected GS-986 doses, plasma IFN-α was detected following GS-986 administration, and was dose-proportional (**figure S3A**).

We next assessed the impact of GS-986 dosing on plasma viremia in monkeys on suppressive ART. The first 3 doses of GS-986 administered to the four SIV-infected ART-suppressed RMs had no effect on plasma viremia. However, further administration induced transient SIV plasma RNA in all RMs (**Fig. 1B**). We detected plasma SIV RNA blips in two animals after the 4th dose, and during doses 5–7 all RMs displayed a moderate level of transient viremia (500-1000 SIV RNA copies/mL). Plasma viremia peaked 24-48 hours after GS-986 exposure and returned to baseline suppression (<50 SIV RNA

copies/mL) within 4-7 days after GS-986 dosing. All vehicle-treated control RMs remained aviremic throughout the study.

To assess the nature of the SIV plasma blips elicited by GS-986, we performed single genome sequencing (SGS) of viral RNA isolated from the blood plasma (during blips), and proviral DNA from peripheral blood mononuclear cells (PBMC), gastrointestinal mucosa mononuclear cells (GMMC) and lymph node mononuclear cells (LNMC), as described(*23*). The sequence of SIV group-specific antigen (*gag)* and SIV envelope (*env*) coding regions isolated during the GS-986-induced plasma blips shared phylogenetic identity to the low diversity, monophyletic sequences prevailing in PBMCs, GMMCs and LNMCs; suggesting that the released virus arose from a reservoir pool established very early after infection (**figure S4A**). Moreover, a significant proportion of the proviral sequences analyzed from blood and tissues isolated from treated and control animals were found to be significantly more diverse than the plasma blip sequences. These proviral sequences were generally phylogenetically distinct from the GS-986-induced plasma viral RNA sequences. Specifically, SIV DNA sequences were found to harbor significant levels of hypermutated defective proviral sequences, implying that the GS-986-induced SIV RNA possibly arose from replication-competent provirus (**figure S4A-B**).

To determine if the *env* genes of the GS-986-induced plasma viruses were infectious, we produced SIV pseudovirion stocks encoding all 11 full-length *env* sequences cloned from GS-986-induced plasma virus blips (n=4) and from *env* sequences isolated from cell-associated proviral DNA (n=7). We then generated SIV-*env* pseudoviruses that were evaluated using a *TZM-bl* based infectivity assay. We found that 3 of 4 plasma virus blip-derived SIV *env* constructs were infectious at levels comparable to wild-type SIVmac251 *env*. Only one *env* gene cloned from the plasma virus blip RNA was non-infectious. All seven *env* sequences cloned from proviral DNA were significantly hypermutated, and thus failed to mediate infection in this assay (**figure S5**).

To further assess the impact of the GS-986 regimen on the viral reservoir, we evaluated SIV DNA levels in sorted CD4+ T cell populations isolated from PBMC, GMMC, and LNMC samples prior to the first exposure (Pre-TLR7) and 1 week after the last dose GS-986 treatment (Post-TLR7).

Specifically, CD4+ T cell subpopulations were sorted into naïve (T_N), central memory (T_{CM}), transitional memory (T_{TM}), and effector memory (T_{EM}). The memory populations were then pooled for SIV DNA measurements. In GS-986-treated RMs, an average reduction of 75% was observed in SIV DNA (**Fig. 2**). SIV DNA remained largely unchanged in the vehicle-treated control RMs. SIV DNA in the CD4+ memory T populations had declined in LNMCs from all four GS-986-treated RMs, and from three of four RMs in PBMC. GS-986 treatment reduced SIV DNA in the GMMC-derived CD4+ T cells in all four treated RMs to undetectable levels (**figure S6**).

Two weeks after the final GS-986 dose, ART was discontinued to determine if GS-986-associated plasma viral blips and reduction in viral DNA would alter SIV rebound kinetics. Rebound viremia occurred in all animals within 7-10 days after stopping ART (**Fig. 3**). We analyzed the kinetics of SIV RNA rebound in the plasma from all 10 RMs through day 84 after stopping ART but did not observe any difference in the time to SIV rebound between GS-986-treated or vehicle-treated control animals. We next assessed viral peak (week 2-3), set-point (week 7-8) and the total viral burden for each RM by calculating the AUC of SIV RNA between days 1 and 56 following ART release. Analyses of all three parameters showed reduced plasma SIV RNA in GS-986-treated animals relative to those of controls, however the differences were not significant (peak, P=0.476; set-point, P=0.171; and AUC, P=0.476, **figure S7A**). We then repeated all statistical tests without the single control animal with unusually low viremia. The differences in both viral peak and AUC between treated and control RMs reached statistical significance (P=0.008 and P=0.02, respectively). The same statistical tests were also conducted adding nine additional historic control animals that received the same SIV stock, dose, and route, and had also initiated ART at day 65 following infection (**figure S7B)**. Importantly, viral kinetics after ART cessation in these additional control RMs did not show a difference in rebound compared to five of the six control animals from Study 1. Viral peak and set-point analyses found a significant median reduction of SIV RNA in GS-986-treated RMs compared to controls (P=0.03 and P=0.04, respectively). Differences in AUC between treated and control RMs also was also statistically significant (P=0.01) (**figure S7C**). This reduction in median set-point viremia in GS-986-treated RMs persisted for the entire 84-day monitoring

period following ART cessation.

In Study 2, we compared the tool analog GS-986, to the clinical TLR7 agonist molecule GS-9620, for the ability to induce transient viremia and reduce the SIV reservoir. We also evaluated two clinically relevant translational endpoints: first, to determine if dose reductions are effective in limiting peripheral IFN-α that, if too high, often result in clinical participants experiencing "flu-like" symptoms; and second, to assess the tolerability and efficacy of an increased number of TLR7 agonist doses. Eleven SIV-infected ART-suppressed RMs were divided into 4 groups based on viral load pre-ART, time to viral suppression after ART initiation, and balanced CD4+, CD8+ and CD4+/CD8+ T cell ratios (**figure S1B**). Group 1 served as placebo controls (n=2) and received formulation vehicle only. Group 2 (n=3) received GS-986 (0.1 mg/kg) and Groups 3 and 4 (n=3/group) received lower (0.05mg/kg) or moderate (0.15mg/kg) doses of GS-9620 (**figure S2B**). All animals received 10 doses of either GS-986 or GS-9620 EOW, followed by a rest period of 3 months, while maintaining ART. After the treatment pause, we resumed dosing in all groups (with the exception of Group 4) for an additional 9 doses at the same dose concentration and frequency.

We monitored the same virologic and immunologic endpoints as in Study 1. In Study 2, the reduced doses of GS-986 and GS-9620 had similar effects in regard to the activation of NK, T and B cells. However, we observed that the 0.1mg/kg doses of GS-986 activated a greater proportion of NK and T cell populations when compared to the 0.15mg/kg GS-9620 concentration.

Interestingly, at the TLR7 agonist doses used, we found that the activation of peripheral blood T cells in the TLR7 agonist-treated RMs was primarily in the effector memory subpopulation ($CD95^+CD28^-$), with limited activation of naïve ($CD95^-CD28^+$) or central memory ($CD95^+CD28^+$) T cell populations (**Fig. 4**). Similarly, specific subpopulations of NK cells defined as $CD16^+$ and $CD16^-CD56^-$ were preferentially activated over $CD16^-CD56^+$ NK cells (**figure S8A**). Conversely, naïve B cells ($CD27^-$) tended to be activated to higher magnitude than memory ($CD27^+$) B cells, as measured by elevated CD38 expression (**figure S8B**).

Consistent with the results observed in Study 1, we found that the repeat dosing of GS-986 or GS-9620 induced transient viremia in all treated RMs (doses 3 through 10), and that viral reactivation was detectable from the 3rd to 10th dose (**Fig. 5**). However, in this second study using lower doses of the TLR7 agonists, the plasma viral blip frequency was reduced and variable. In each monkey, we analyzed the total amount of SIV RNA released in the plasma within 72 hours after each TLR7 agonist dose by calculating the AUC. Total plasma SIV RNA levels (in both studies) peaked after the 5th TLR7 agonist dose, and declined thereafter (**figure S9**). After 10 doses of GS-986 and GS-9620, all RMs underwent a 3-month pause without TLR7 agonist dosing. We then resumed vehicle, GS-986 or GS-9620 (0.05 mg/kg) dosing for an additional 9 doses, again EOW. Similar to the first phase of Study 2, rapid activation of T, B and NK cell subsets was observed **(Fig**. **4, figure S8A-B**). Interestingly, during the second phase of dosing, only a single viral blip was observed in one animal.

Motivated by the findings of Study 1, SIV DNA levels were again quantified and showed a reduction in CD4+ memory T cells from all TLR7 agonist-treated RMs, yet minimally changed in control animals (**Fig. 6A**). Repeated TLR7 agonist dosing was associated with viral DNA reductions in the blood and tissues; this trend was not observed in control animals. The most significant decrease in SIV-DNA levels were observed in either T_{TM} or T_{EM} subsets in most RMs treated with TLR7 agonists (**Fig. 6B**). Importantly, SIV DNA in T_{CM} was variable in most TLR7 treated RMs, however, there was a significant reduction in this value measured in T_{CM} from two RMs.

We then conducted a combined statistical analysis for all TLR7 agonist-treated RMs. Significant reductions in SIV DNA in both PBMC (0.79 log median, P=0.004) and GMMC (0.33 log median, P=0.027) were detected, while a strong trend towards significance in LNMC was also observed (0.33 log median, P=0.054) (**figure S6**).

Plasma IFN-α concentrations were also analyzed in all animals from Study 1 and 2 (**figure S3B**). In the first study, all four RMs treated with increasing doses of GS-986 had detectable plasma IFN-α at 24 hours after each dose. As expected, in the second study using reduced pharmacodynamic doses of the TLR7 agonists, only one animal (receiving 0.1 mg/kg GS-986) out of all 9 TLR7 agonist-treated animals

had appreciable plasma IFN-α in the initial 10 doses. Intriguingly, in the subsequent 9 doses, after the 3-month rest period, there was transient but detectable induction of IFN-α with the greatest changes in animals receiving 0.1 mg/kg GS-986 as compared to the initial 10 doses. (**figure S3B**).

To confirm that the TLR7 agonists were eliciting biological activity in Study 2, we evaluated expression of the interferon-stimulated gene (ISG) mRNAs ISG15, Mx1 and OAS1. All animals treated with a TLR7 agonist showed transient dose-dependent induction of all three ISG mRNAs (**figure S10**). The peak induction of each ISG mRNA in the GS-986 and GS-9620 (0.15 mg/kg) dose groups was within 24h. The GS-986 group showed the most robust induction of ISGs. However, these returned to baseline with 72 hours or before the next dose.

We also assessed the pattern of cytokine expression resulting from TLR7 agonist administration in both studies. In Study1, where animals received increasing IFN-α-inducing doses of GS-986, multiple plasma cytokines and chemokines were transiently produced following administration of the TLR7 agonist that were found to be proportional to dose. Peak production of cytokines and chemokines with the exception of RANTES, was observed in most RMs within 24-48 hours after GS-986 dosing (**figure S11A**). The most robustly induced plasma cytokine following TLR7 agonist treatment in this study was interleukin-1 receptor antagonist (IL-1RA), a marker of immune activation and regulation. Interferon–inducible T Cell Alpha Chemoattractant (I-TAC) was also readily inducible by each TLR7 dose. The rise in concentration of both IL-1RA and I-TAC after 24h post each TLR7 agonist dose was significant compared to baseline (**figure S11A and B**).

In Study 2, we found that treatment with GS-986 or GS-9620 (0.15 mg/kg) transiently induced cytokines (or chemokines), but RMs receiving the lower GS-9620 dose (0.05 mg/kg) had very low or undetectable plasma cytokine concentration demonstrating that cytokine production was proportional to GS-9620 dose (**figure S11C**). Consistent with Study 1, IL-1RA and I-TAC were highly induced following TLR7 agonist treatment. Interestingly, in the subsequent 9 doses, after the 3-month rest period, although there was weak induction of IL-1RA after each TLR7 dose, overall fold changes were

significantly decreased in animals receiving 0.1 mg/kg GS-986 compared to the initial 10 doses (**figure S11D**).

To assess changes in the size of the inducible SIV reservoir longitudinally after TLR7-agonist treatment, we used a modified *in vitro* viral outgrowth assay (see Methods) amenable to the limitations in blood draw volumes in RMs. PBMC were isolated from RMs before and after treatment, and LNMC from post-treatment, and were activated *in vitro* using Concanavalin A (ConA). Six days after activation, SIV RNA was isolated from culture supernatants and quantified by RT-PCR.

We observed longitudinal reductions in the amount of reactivated SIV produced from PBMCs isolated from most TLR7-agonist treated animals (**Fig. 6C**). However, SIV RNA produced from control RMs remained essentially unchanged over time. Importantly, two TLR7 agonist treated RMs, animals 177-10 (GS-9620 0.15 mg/kg group) and 344-10 (GS-986 0.1 mg/kg group), were completely negative for ConA-induced SIV RNA induction in both PBMC and LNMC samples taken after the 10^{th} and 19^{th} TLR-7 agonist dose, respectively.

To assess if these reductions in the cell-associated SIV reservoir were predictive of viral rebound, ART was discontinued for all Study 2 animals. Rebound occurred in most RMs within 7-10 days of ART release (**Fig. 6D**). Strikingly, the same two RMs, which were negative in both PBMC and LNMC for ConA-inducible SIV, did not rebound. In both animals, plasma viremia has remained undetectable for more than 700 days after stopping ART, at the time of this report. We also observed that two viremic RMs from TLR-7 agonist treated groups showed continual decline in their plasma viral RNA after day 100 to the time of this report.

To address if this absence of rebound viremia was a result either of immune control or reservoir clearance, we conducted a series of *in vitro* experiments. We first evaluated the development of anamnestic T cell responses following ART release by measuring the frequency of virus-specific cytokine-producing T cells on the day of ART release (day 0) and on days 35 and 177 after ART stop. RMs that had recrudescent viremia developed clear anamnestic SIV-specific T cell responses, whereas aviremic RMs did not respond to SIV-peptide stimulation (**figure S12**).

We next performed an *in vitro* viral outgrowth assay using PBMCs isolated at day 177 post ART stop from two aviremic RMs (177-10 and 344-10), and also from two viremic RMs (162-09 and 305-10) to serve as positive controls. After six days of stimulation, virus was readily detectable in PBMCs from viremic animals, yet RMs 177-10 and 344-10 remained completely negative (**figure S13A**).

We next assessed if SIV could be cultured from the PBMC, and initiate infection in CEMx174 cells in the absence of CD8+ T cells. We co-cultured $1x10^6$ CD8+ T cell-depleted PBMC with $5x10^6$ CEMx174 cells. Virus production in culture supernatants was monitored by RT-PCR of samples taken on days 5, 9 and 14 after co-culture. We were unable to detect virus from PBMCs isolated from the two aviremic RMs; whereas PBMC from the two viremic RMs initiated high-level viral replication in CEMx174 cells (**figure S13B)**.

To determine if any replication-competent virus remained in our remission animals, we performed an *in vivo* antibody-mediated depletion of CD8+ lymphocytes in both aviremic RMs (177-10 and 344-10), and two viremic RMs (288-10 and 295-10). Post-infusion, *in vivo* CD8+ lymphocytes were rapidly depleted, in all RMs, by three days after antibody treatment (**figure S14** and **Fig. 7A**), and CD8+ cells were completely cleared from the peripheral blood for at least 17 days. In the absence of CD8+ cells, the 2 viremic RMs displayed a rapid spike in plasma viral RNA levels. However, neither aviremic RM had any detectable plasma virus at any point during CD8+ lymphocyte depletion (**Fig. 7A**).

Finally, to confirm whether the lack of detectable viremia in our remission animals was due to the clearance of replication competent SIV or immune mediated viral suppression, we performed adoptive cell transfer studies (as described in Methods). In two separate transfer experiments, we infused samples obtained before or after TLR7 treatment into four naïve RMs (n=2/group). In the first transfer, we used approximately 50 million frozen PBMC and LMNC obtained from each animal (i.e. 177-10 and 344-10) post-ART, just prior to TLR7-agonist treatment. PBMC and LNMC from each respective RM were combined, then infused into a single naïve recipient macaque, and readily initiated *de novo* infection by day 7 following transfer (**Fig. 7B**). In the second transfer, fresh PBMC and LN from day 448 post-ART release, were isolated within 2 hours from biopsy for each remission RM (177-10 and 344-10). These

fresh PBMC and LMNC mixtures from each aviremic RM were transfused into one naïve recipient RM, respectively. Despite infusion of more than 120 million fresh PBMC and LMNC from each aviremic RM, we failed to initiate infection into either naïve recipient macaque (**Fig. 7B**). These latter two recipient RMs were monitored for 28 days post-infusion, with no evidence of detectable viremia.

We next used viral dynamics modeling to gain further insight into the effects of treatment with TLR7-agonist therapy (**figure S15A**). We found no significant differences in either set-point viremia or time to rebound between treatment and control animals in either study (**figure S15B**). However, examining the kinetics of rebound after ART-cessation, we found that the TLR7 agonist-treated monkeys that rebounded showed decreased viral reactivation rates (Study 1 $p=0.03$, Study 2 $p=0.05$, pooled $p=0.01$) and increased viral growth rates ($p=0.02$, $p=0.05$, and $p=0.03$) compared to a pooled control group (**figure S15C-D**). A summary of the differences in rebound kinetics between treated and control RMs are shown (**figure S15E-F**). Our analysis suggests that TLR7 agonist treatment may have reduced the reservoir even in RMs who did rebound after ART removal.

We also predicted the distribution of rebound times as a function of the reduction in the reservoir size, using a separate stochastic model of viral reactivation and rebound. Survival curves show the predicted percentage of animals that have not yet rebounded as a function of time after ART cessation (**figure S15G**). For the two aviremic RMs, we used this model to estimate that the reservoir had been reduced more than 1400–fold by TLR7 agonist treatment (95% CI [110, 32 000]) to explain a greater than two-year delay in SIV rebound, assuming reservoir reduction was the sole mechanism for control of any recrudescent viremia (**figure S15H**). Given that CD8+ lymphocyte depletion did not lead to loss of viral control in these animals, and adoptive transfer of cells did not induce viremia in naïve recipients, we believe this is reasonable. Furthermore, modeling of cumulative viral blip trajectories suggested that the viral blip sizes induced by TLR7-agonist treatment were compatible with meaningful reductions in the size of the latent reservoir (i.e. ~ 1% of all SIV DNA+ cells reactivated over the whole treatment course). Model fit parameters for individual animals are shown in (**figure S16**).

Discussion

We demonstrate in two independent RM studies, the ability of TLR7 agonist exposure to induce potent immune responses along with an increase in select interferon-regulated antiviral genes and cytokines. Similarly, TLR7 agonist treatment induced transient viremia that was concurrent with immune activation. Ultimately, the combination of TLR7 agonist-induced immune potentiation and transient viremia may have resulted in the observed reductions in the viral reservoir in our non-human primate model for HIV latency.

Importantly, in these studies we have used a stringent animal model, involving a pathogenic SIVmac251 strain and have excluded RMs with MHC alleles known to confer enhanced SIV control, which we believe enhances the significance of our findings. The proportion of RMs that could be expected to spontaneously control SIV after ART discontinuation has not been previously determined statistically; however, not a single case of viral remission has been observed by our group in MHC-defined (A*01-, B*08-, B*17-negative) RMs starting ART relatively late (at day 65 following SIVmac251 infection) or even in groups of RMs administered ART as early as day 3 post-infection, where the reservoir is significantly smaller(*22*).

Despite the stringency of our RM persistence model, there are notable limitations to the present study. Several practical considerations limited the numbers of RMs used for treatment and control arms, thus the overall power to discriminate significance in certain analyses may be reduced. SIV-infected animals on ART are similar, but certainly not identical, to HIV-infected participants on ART therapy, with notable differences between viruses and between organisms. One important difference is that study participants have typically been maintained on potent ART regimens for significantly longer periods than were achieved in this study. These extended periods of ART treatment in human participants are expected to have an impact on the HIV-1 reservoir.

Our data show that TLR7 agonists exhibit biological effects *in vivo* that are consistent with the induction of transient viremia and SIV DNA reductions in most animals after agonist exposure. However, the precise mechanism(s) by which these TLR agonists induce transient viremia remains to be fully

defined. We have identified several biologic correlates that hallmark this phenomenon, and we posit that these cytokine signatures, in concert with repeated TLR7 agonist-induced activation of CD4+ T memory subsets, led to the induction of SIV detected in the plasma.

Dosing of the TLR7 agonists was well tolerated throughout both studies. As each TLR7 agonist was orally-dosed, exposure in the gut was expected to be higher, possibly leading to enhanced activation in these tissues. Specifically, formulated TLR7 agonist adsorption and effect are expected to be proportionally higher in the gut, as both agonist compounds possess high absorption properties in the gastrointestinal (GI) tract and only moderate clearance rates during the first-phase of hepatic metabolism. While these properties limit systemic exposure of TLR7 agonists following oral administration, they enhance drug exposure in the GI tract and the liver(*18, 19, 24*). Therefore, it is not surprising that the effects of these agonists appeared to be enhanced in the gut, as observed in the reduction of SIV DNA in CD4+ T cells from GMMC. This latter observation is also consistent with the significant increases in IL-1RA observed after each TLR7 agonist exposure, signifying high cellular activation in the gut. Thus, it seems plausible that a proportion of the viremia that was detected after TLR7 agonist exposure may have arisen, at least initially, from this compartment. Unfortunately, our sequence analysis could not discriminate a tissue-specific SIV sequence to confirm this possibility. However, the modulation of IL-1RA in both studies serves as a potential biomarker. The modulation of this cytokine is broadly concordant with the enhanced clearance of provirus from the GMMC in most animals, and particularly those receiving higher treatment concentrations.

We also show a strong association of I-TAC (CXCL11) that parallels the induction of transient viremia, and the observed immune activation and presumed effector recruitment to multiple (reactivated) sites of infection, including the lymph nodes(*25*). In this context, I-TAC may also serve as a signature or "trigger" cytokine for the induction of transient viremia. Indeed, a positive correlation has been observed between GS-9620- induced peak of IP-10 (CXCL10), I-TAC (CXCL11) and HIV re-activation levels *in vitro*. However, we cannot discount the role of other innate and adaptive mediators, potentiated by TLR7 agonist exposure, in the induction of viremia. These same responses may have aided the clearance of re-

activated SIV-infected cells.

As abovementioned, these biologic effects appear consistent with the potential to reduce viral DNA during ART, although complete remission was observed only in a subset of animals after ART discontinuation. In the two aviremic RMs, it is noteworthy that durable remission was only achieved with a complete clearance of *in vitro* inducible virus from both the PBMC and LNMC. Animals that had otherwise displayed significant reservoir reductions (in the blood, LN or gut) but had any inducible SIV in the lymph nodes, recrudesced once ART was discontinued. These "rebounder" observations were predicted based on our modeling analysis. However, many of the TLR7-treated RMs that exhibited viral rebound, also showed longitudinal reductions in viral setpoint as evidence of therapeutic effect.

A detailed assessment of the virologic and immunologic differences between viremic and remission RMs following TLR7 agonist administration revealed significant reductions in SIV-DNA in T_{CM} and T_{TM} populations from PBMC and T_{CM} from LNMC. These SIV DNA reductions in memory subsets were concurrent with significant increases of I-TAC during TLR7 agonist doses 1 through 10 and proportional increases in mRNA expression of ISG15 and Mx1. Although these ISGs were induced in all RMs following TLR7 agonist treatment (in a dose-response manner), increased expression of both ISG15 and Mx1were noted in the RMs that ultimately became aviremic.

Therefore, our model predictions of cumulative viral reactivation events suggest that repeated episodes of transient viremia induced by TLR7-agonist treatment are consistent with the observed reductions in the latent reservoir and help to explain the now greater than 24-month period of undetectable SIV in two RMs. As abovementioned, this prediction assumes reservoir reduction is the sole mechanism for lack of recrudescent viremia. The possibility of this being true is partially corroborated by several observations favoring SIV clearance as the dominant mechanism over immunologic suppression. First, remission animals exhibit no SIV-specific cellular immune responses following release of ART. Second, long-term CD8+ lymphocyte depletion did not result in any recrudescent viremia. Third, the adoptive transfer of cells (PBMC and LNMC) from aviremic RMs did not induce viremia in naïve recipients. Fourth, neutralizing antibodies could have afforded some level of control. However, antibody

profiles were evaluated and had waned to undetectable levels in most animals during ART, as expected (*26*). Neutralizing antibody was also assessed at various times after ART release and neither remission RM mounted any detectable neutralizing responses post-ART cessation. Finally, a sustained viral remission of greater than two years, absent ART and an immune correlate of control, could only be sustained by a near-complete clearance of all the replication-competent viral reservoir. Therefore, we believe our assumption favoring SIV reservoir reduction is reasonable, but likely requires additional confirmatory experimentation.

In conclusion, these findings support the further evaluation of TLR7 agonists, their impact on the viral reservoir, and possible use in combination with other viral eradication strategies.

Acknowledgements

We thank J. Harrison, C. Gittens, J. Yalley-Ogunro, H. Anderson and W. Wagner for expert animal husbandry and care. CD8 depleting antibody, MT807R1 and anti-CD38-PE was obtained from the NIH Nonhuman Primate Reagent Resource supported by HHSN272200900037C and OD010976. We acknowledge support from Gilead Sciences and the National Institutes of Health; NIAID award AI126617, co-funded by NIDA, NIMH, NINDS; DP5OD019851 awarded to A.L.H. and NIAID grants AI091514, AI122942, AI127089 and AI131365 awarded to J.B.W.

Author Contributions

J.H., T.C., M.D.M., R.G., W.A.L. and J.B.W. designed the studies. S.S, C.E.O., M.S. and S.Y.L. led the virologic assays and viral sequencing. S.S., S.Y.L. and C.E.O. led the immunologic assays. J.H., T.L.B. and SY.L. led the cytokine and chemokine analysis. P.T.H. led the bioinformatics analysis. A.L.H. and J.M.G. led the mathematical modeling. J.B.W and M.G.L led the interventions and clinical care of the rhesus monkeys. J.B.W. led the studies and wrote the paper with all co-authors.

Author Information

J.H., R.G., T.C., M.D.M., and W.A.L. are employees of Gilead Sciences and own stock and/or stock options of Gilead Sciences. All other authors declare no competing financial interests.

Correspondence should be addressed to J.B.W. (jwhitne2@bidmc.harvard.edu).

Figure Legends

Figure 1. Modulation of lymphocyte activation during oral GS-986 dose escalation (A). Activation of lymphocyte subsets in the peripheral blood was monitored by flow cytometric detection of CD69 on (from the top): $CD4^+$ T cells, $CD8^+$ T cells, NK cells, and B cells. CD69 expression was measured at pre-GS-986 dose and at 24, 48, 72, and 168 hours after treatment. Shown are the absolute differences in percent $CD69^+$ cells from time of treatment, for each of seven doses. Bar height indicates mean difference. Error bars, SEM. **Transient plasma viremia induced by TLR7 agonist dosing in SIV-infected monkeys on ART (Study 1) (B).** Plasma SIV RNA copies in RMs following a single oral dose of TLR7 agonist every other week is shown. RMs (n=4) were treated with escalating doses of GS-986 over 14 study weeks. Dose concentrations were 0.1mg/kg, 0.2mg/kg and then five consecutive doses at 0.3mg/kg, given orally every other week. The control group received formulation vehicle only (n=6).

Figure 2. Effect of TLR7 agonist on cell-associated viral DNA in CD4+ T memory cells.

PBMC, inguinal LNMC and GMMC were collected prior to the administration of TLR7 agonist (Pre-TLR7) and one week after the 7^{th} dose of GS-986 (Post-TLR7). Mononuclear cells were isolated from each tissue and sorted into four populations of CD4+ T cells: naïve, central memory (CM), transitional memory (TM) and effector memory (EM). Memory subsets were then pooled, as described in Methods. SIV DNA in the pooled memory populations are expressed as $\log_{10}$ copies per 10^6 cells. Threshold of detection, as indicated by the dotted line, is <3 copies per 10^6 cells.

Figure 3. The kinetics of SIV plasma RNA rebound after ART cessation. Log plasma virus RNA was assessed in SIV-infected RMs between days 1 to 84 following ART cessation. Median $\log_{10}$ SIV RNA copies/mL for GS-986 treated (—) and control (—) animals is shown relative to ART stop (Day 0).

Figure 4. Effector memory T cells are preferentially activated by TLR agonists (Study 2). Activation of naïve ($CD95^-CD28^+$), central memory ($CD95^+CD28^+$), and effector memory ($CD95^+CD28^-$) $CD4^+$ (**A**)

and $CD8^+$ (**B**) T cells in the peripheral blood of vehicle (—), GS-986 (0.1mg/kg) (—), GS-9620 (0.05mg/kg) (—), and GS-9620 (0.15mg/kg) (—) treated monkeys was monitored by flow cytometric detection of CD69. CD69 expression within each subset was measured at time of dose and at 24, 48, and 72 (doses 1-7 only) hours post-dose (time points indicated by x-axis ticks) for doses 1, 3, 5, and 7 (**left**) and doses 11-19 (**right**). Shown are the changes in percent $CD69^+$ cells from day of dose, for each dose.

Figure 5. **Transient plasma viremia induced by TLR7 agonist dosing in SIV-infected monkeys on ART (Study 2).** Animals were treated with placebo (n=2), GS-986 0.1 mg/kg (n=3), GS-9620 0.05 mg/kg (n=3), or GS-9620 0.15 mg/kg (n=3) over 23 study weeks. Plasma viral RNA in vehicle-treated or TLR7 agonist dosed animals are shown. Arrows indicate the timing of each TLR7 agonist dose. The horizontal dotted line represents the limit of detection of plasma viremia.

Figure 6. Changes in cell-associated viral DNA in mononuclear cells isolated from tissue compartments in monkeys treated with TLR7 agonist (Study 2) (A). Mononuclear cells were isolated from tissues of animals treated with either vehicle, 0.1mg/kg of GS-986, 0.05mg/kg or 0.15mg/kg of GS-9620 and sorted into four populations of CD4+ T cells: naïve, central memory (CM), transitional memory (TM) and effector memory (EM), then memory subsets were pooled in order to increase sensitivity for DNA analysis, as described in Methods. SIV DNA is expressed as $\log_{10}$ copies per 10^6 CD4+ T memory cells at the time of the administration of TLR7 agonist (Pre-TLR7), and a week prior to stopping ART (Pre-ATI). **SIV DNA in each subpopulation of CD4+ T cells in TLR7 treated RMs combined at pre- and post-TLR7 agonist treatment (B).** The threshold of detection, as indicated by the horizontal line, is <3 copies per 10^6 CD4+ T cells. Changes in SIV DNA between pre- and post-treatment was compared using a Wilcoxon matched paired test. ***Ex vivo*** **mitogen-stimulated virus production assay (C).** PBMC or LNMC (post-19^{th} dose only) were isolated from monkeys prior to the administration of the first dose of TLR7 agonist (Pre-TLR7), then after the 10^{th} and 19^{th} doses. Cells were cultured in basal medium

supplemented with 10mM raltegravir, with or without ConA (5 µg/mL) for 6 days. SIV RNA copies/ml of supernatant on day 6 are shown.

SIV plasma RNA rebound kinetics after stopping ART in Study 2 monkeys (D). The viral rebound kinetics after stopping ART were assessed in groups of RMs treated with either vehicle (control), GS-986 (0.1 mg/kg) or GS-9620 (0.05 mg/kg or 0.15 mg/kg). Log plasma virus RNA was assessed between days 1 to 210 following ART cessation. **CD8+ lymphocyte concentrations and SIV plasma RNA kinetics following *in vivo* CD8+ lymphocyte depletion (E)**. CD8+ lymphocytes were depleted *in vivo* by monoclonal antibody infusion (MT807R1) and frequencies per µL whole blood were monitored by flow cytometry. Log plasma virus RNA was assessed between days 0 to 35 post-depletion. **Adoptive transfer studies in naïve macaques (F).** Four SIV naïve rhesus macaques were used for adotive transfer of cells from remission animals (n=2/grp). In the first transfer, approximately 50 million frozen PBMC and LNMCs from animals 177-10 and 344-10, isolated after the initiation of ART but prior to TLR7 agonist treatment, were used for adpotive transfer. For each donor PBMC and LMNC were thawed, combined, and then infused into 2 naïve RMs (177-10, ; 344-10,). In the second transfer, approximately 120 million fresh PBMC and LMNC from each donor were isolated at 448 days after ART stop. PBMC and LMNC were combined and then infused fresh into two additonal naïve RMs (177-10, ; 344-10,). Log plasma virus RNA was assessed between days 0 to 28 post-adoptive transfer.

References

1. D. Finzi *et al.*, Latent infection of CD4+ T cells provides a mechanism for lifelong persistence of HIV-1, even in patients on effective combination therapy. *Nature medicine* **5**, 512-517 (1999).
2. D. Finzi *et al.*, Identification of a reservoir for HIV-1 in patients on highly active antiretroviral therapy. *Science (New York, N.Y.)* **278**, 1295-1300 (1997).
3. R. T. Gandhi *et al.*, The effect of raltegravir intensification on low-level residual viremia in HIV-infected patients on antiretroviral therapy: a randomized controlled trial. *PLoS Med* **7**.
4. D. M. Margolis, Eradication therapies for HIV Infection: time to begin again. *AIDS Res Hum Retroviruses* **27**, 347-353.
5. D. M. Margolis, Mechanisms of HIV latency: an emerging picture of complexity. *Curr HIV/AIDS Rep* **7**, 37-43.
6. N. M. Archin *et al.*, Expression of latent HIV induced by the potent HDAC inhibitor suberoylanilide hydroxamic acid. *AIDS Res Hum Retroviruses* **25**, 207-212 (2009).
7. N. M. Archin *et al.*, Valproic acid without intensified antiviral therapy has limited impact on persistent HIV infection of resting CD4+ T cells. *Aids* **22**, 1131-1135 (2008).
8. N. M. Archin *et al.*, Antiretroviral intensification and valproic acid lack sustained effect on residual HIV-1 viremia or resting CD4+ cell infection. *PLoS One* **5**, e9390.
9. G. K. Sahu, M. W. Cloyd, Latent HIV in primary T lymphocytes is unresponsive to histone deacetylase inhibitors. *Virol J* **8**, 400.
10. K. S. Keedy *et al.*, A limited group of class I histone deacetylases acts to repress human immunodeficiency virus type 1 expression. *J Virol* **83**, 4749-4756 (2009).
11. S. Xing *et al.*, Disulfiram reactivates latent HIV-1 in a Bcl-2-transduced primary CD4+ T cell model without inducing global T cell activation. *J Virol* **85**, 6060-6064.
12. S. Matalon, T. A. Rasmussen, C. A. Dinarello, Histone deacetylase inhibitors for purging HIV-1 from the latent reservoir. *Mol Med* **17**, 466-472.
13. J. C. Burnett *et al.*, Combinatorial latency reactivation for HIV-1 subtypes and variants. *J Virol* **84**, 5958-5974.
14. K. Huber *et al.*, Inhibitors of histone deacetylases: correlation between isoform specificity and reactivation of HIV type 1 (HIV-1) from latently infected cells. *J Biol Chem* **286**, 22211-22218.
15. R. B. Jones *et al.*, Histone deacetylase inhibitors impair the elimination of HIV-infected cells by cytotoxic T-lymphocytes. *PLoS pathogens* **10**, e1004287 (2014).
16. N. G. Sandler *et al.*, Type I interferon responses in rhesus macaques prevent SIV infection and slow disease progression. *Nature* **511**, 601-605 (2014).
17. S. Menne *et al.*, Sustained efficacy and seroconversion with the Toll-like receptor 7 agonist GS-9620 in the Woodchuck model of chronic hepatitis B. *Journal of hepatology* **62**, 1237-1245 (2015).
18. R. E. Lanford *et al.*, GS-9620, an oral agonist of Toll-like receptor-7, induces prolonged suppression of hepatitis B virus in chronically infected chimpanzees. *Gastroenterology* **144**, 1508-1517, 1517.e1501-1510 (2013).
19. U. Lopatin *et al.*, Safety, pharmacokinetics and pharmacodynamics of GS-9620, an oral Toll-like receptor 7 agonist. *Antiviral therapy* **18**, 409-418 (2013).
20. D. H. Barouch *et al.*, Vaccine protection against acquisition of neutralization-resistant SIV challenges in rhesus monkeys. *Nature* **482**, 89-93 (2012).

21. N. L. Letvin *et al.*, Immune and Genetic Correlates of Vaccine Protection Against Mucosal Infection by SIV in Monkeys. *Sci Transl Med* **3**, 81ra36 (2011).
22. J. B. Whitney *et al.*, Rapid seeding of the viral reservoir prior to SIV viraemia in rhesus monkeys. *Nature* **512**, 74-77 (2014).
23. J. B. Whitney *et al.*, Genital tract sequestration of SIV following acute infection. *PLoS pathogens* **7**, e1001293 (2011).
24. A. Fosdick *et al.*, Pharmacokinetic and pharmacodynamic properties of GS-9620, a novel Toll-like receptor 7 agonist, demonstrate interferon-stimulated gene induction without detectable serum interferon at low oral doses. *The Journal of pharmacology and experimental therapeutics* **348**, 96-105 (2014).
25. J. F. Foley *et al.*, Roles for CXC chemokine ligands 10 and 11 in recruiting CD4+ T cells to HIV-1-infected monocyte-derived macrophages, dendritic cells, and lymph nodes. *J Immunol* **174**, 4892-4900 (2005).
26. K. Dreyer *et al.*, Primary isolate neutralization by HIV type 1-infected patient sera in the era of highly active antiretroviral therapy. *AIDS Res Hum Retroviruses* **15**, 1563-1571 (1999).
27. L. J. Yant *et al.*, The high-frequency major histocompatibility complex class I allele Mamu-B*17 is associated with control of simian immunodeficiency virus SIVmac239 replication. *J Virol* **80**, 5074-5077 (2006).
28. B. R. Mothe *et al.*, Expression of the major histocompatibility complex class I molecule Mamu-A*01 is associated with control of simian immunodeficiency virus SIVmac239 replication. *J Virol* **77**, 2736-2740 (2003).
29. J. T. Loffredo *et al.*, Mamu-B*08-positive macaques control simian immunodeficiency virus replication. *J Virol* **81**, 8827-8832 (2007).
30. D. Kuhrt *et al.*, Naive and memory B cells in the rhesus macaque can be differentiated by surface expression of CD27 and have differential responses to CD40 ligation. *Journal of immunological methods* **363**, 166-176 (2011).
31. R. L. Webster, R. P. Johnson, Delineation of multiple subpopulations of natural killer cells in rhesus macaques. *Immunology* **115**, 206-214 (2005).
32. R. K. Reeves *et al.*, CD16- natural killer cells: enrichment in mucosal and secondary lymphoid tissues and altered function during chronic SIV infection. *Blood* **115**, 4439-4446 (2010).
33. C. J. Pitcher *et al.*, Development and homeostasis of T cell memory in rhesus macaque. *J Immunol* **168**, 29-43 (2002).
34. J. B. Whitney *et al.*, T-cell vaccination reduces simian immunodeficiency virus levels in semen. *J Virol* **83**, 10840-10843 (2009).
35. J. J. Mattapallil *et al.*, Massive infection and loss of memory CD4+ T cells in multiple tissues during acute SIV infection. *Nature* **434**, 1093-1097 (2005).
36. E. E. Giorgi *et al.*, Estimating time since infection in early homogeneous HIV-1 samples using a poisson model. *BMC bioinformatics* **11**, 532 (2010).
37. B. F. Keele *et al.*, Identification and characterization of transmitted and early founder virus envelopes in primary HIV-1 infection. *Proceedings of the National Academy of Sciences of the United States of America* **105**, 7552-7557 (2008).
38. F. Rodriguez, J. L. Oliver, A. Marin, J. R. Medina, The general stochastic model of nucleotide substitution. *Journal of theoretical biology* **142**, 485-501 (1990).

39. Z. Yang, Maximum likelihood phylogenetic estimation from DNA sequences with variable rates over sites: approximate methods. *Journal of molecular evolution* **39**, 306-314 (1994).
40. J. E. Schmitz *et al.*, Control of viremia in simian immunodeficiency virus infection by CD8+ lymphocytes. *Science (New York, N.Y.)* **283**, 857-860 (1999).
41. J. E. Schmitz *et al.*, A nonhuman primate model for the selective elimination of CD8+ lymphocytes using a mouse-human chimeric monoclonal antibody. *The American journal of pathology* **154**, 1923-1932 (1999).
42. M. M. Donaldson *et al.*, Optimization and qualification of an 8-color intracellular cytokine staining assay for quantifying T cell responses in rhesus macaques for pre-clinical vaccine studies. *Journal of immunological methods* **386**, 10-21 (2012).

Methods

Study Design. These experiments were designed to investigate whether the administration of TLR7 agonist could perturb an established latent reservoir in SIV-infected rhesus macaques on ART. Twenty-one Indian-origin, outbred, young adult, male specific pathogen-free (SPF) rhesus monkeys (*Macaca mulatta*) that did not express the class I alleles *Mamu-A*01*, *Mamu-B*08*, and *Mamu-B*17* associated with enhanced virologic control were housed at Bioqual(*27-29*). Animals utilized for the studies were infected using a repeated low-dose intrarectal challenge with SIVmac251. Animals were assigned to individual study arms to balance the following parameters across groups: 1-pre-ART viral burden; 2- SIV viral load at ART initiation; 3- CD4+, CD8+ T cell count; CD4+/CD8+ ratio and 4- animal weight. **ART regimen.** The pre-formulated antiretroviral therapy (ART) cocktail contained two reverse transcriptase inhibitors, 20mg/mL tenofovir (TFV) and 50mg/mL emtricitabine (FTC) plus 2.5mg/mL of the integrase inhibitor dolutegravir (DTG). This ART cocktail was administered once daily at 1 mL/kg body weight via the subcutaneous route as described. **TLR7 agonists.** GS-986 and GS-9620 were provided by Gilead Sciences. All TLR7 agonist preparations were endotoxin free. Various formulated concentrations of GS-986 or GS-9620 were administered to monkeys every other week at the dose concentrations described. Monkeys were bled up to four times per week to assess immunologic parameters or viral RNA levels. Tissues including lymph node and colorectal mucosa were biopsied prior to, and after the last dose to measure cell-associated provirus. Two weeks after the last dose, ART was discontinued in all groups to monitor viral rebound.

We included all animals in all analyses and confirmed all experimental findings. Technical staff were blinded during data acquisition and un-blinded for data analysis. With 21 monkeys utilized in this study, we had at least 80% statistical power with one-sided type I error of 5% to detect an effect (measurable viral reactivation and alteration from an established baseline of SIV reservoir in blood and tissues) of 80% or greater in animals tested. The animal studies described have been approved by the appropriate Institutional Animal Care and Use Committee (IACUC).

Lymphocyte staining. PBMCs were isolated by Ficoll density gradient centrifugation. Approximately 0.5 x 10^6 PBMC were stained with each of the following 3 panels of antibodies. For the NK cell panel: CD3 (SP34-2), CD8 (SK1), NKG2A (Z199, Beckman Coulter), CD16 (3G8), CD56 (N901, Beckman Coulter), CD69 (TP1.55.3, Beckman Coulter). For the B cell panel: CD3, CD20 (L27), CD38 (OKT10, Nonhuman Primate Reagents Resource Program), CD40 (5C3), CD69, CD95 (DX2), CD27 (O323, eBioscience), and CD86 (2331 (FUN-1)). For the T cell panel: CD3, CD4 (L200), CD8, CD14 (M5E2), CD95 (DX2), CD28 (CD28.2, eBioscience), CD69, and CD20. All antibodies are from BD Biosciences unless otherwise indicated. **Lymphocyte analysis.** All events were gated first on FSC singlets and then lymphocytes. B cells were identified as $CD3^-CD20^+$ and CD27 was used to define naïve ($CD27^-$) and memory ($CD27^+$) subsets (*30*). NK cells were identified as $CD3^-CD8^+NKG2A^+$ and CD16 and CD56 were used to define subsets (*31, 32*). $CD4^+$ and $CD8^+$ T cells were identified as $CD3^+CD14^-$ and CD28 and CD95 were used to define subsets (*33*). CD69 was measured as a percent of lymphocyte population of interest. CD38 was measured as the geometric mean fluorescence (GMF) of the total cell population of interest. To account for any technical fluctuations in fluorescence (such as inconsistent amount of antibody used or unexpected changes in cytometer measurements), CD38 GMF was normalized by dividing by the background CD38 (PE) GMF of a CD38-negative population in the corresponding sample.

Proviral DNA assays. Lymph node and gastrointestinal mucosal biopsies were processed as single cell suspensions essentially as previously described(*22*). Tissue-specific proviral DNA was quantitated as previously reported(*34*). Total cellular DNA was isolated from 5x10^6 cells using a QIAamp DNA Blood Mini kit (Qiagen). The absolute quantification of viral DNA in each sample was determined by qPCR using primers specific to a conserved region SIVmac239. All samples were directly compared to a linear virus standard and the simultaneous amplification of a fragment of human GAPDH gene. The sensitivity of linear standards was compared against the 3D8 cell line as a reference standard as described(*35*). All PCR assays were performed with 100 and 200 ng of sample DNA.

$CD4^+$ T cell memory subset sorting. Cryopreserved samples of PBMC, lymph node, and colorectal biopsies were thawed at 37°C in RPMI 1640 containing 10% FBS and benzonase (Millipore) at 50U/mL. Cells were re-suspended in 1X PBS containing Aqua LIVE/DEAD Fixable Dead Cell Stain (Life Technologies) for 20min at RT in the dark. Cells were washed and re-suspended in wash buffer containing the following fluorescently-conjugated antibodies: CD45 (D058-1283), CD28 (CD28.2 Beckman Coulter), CD4 (L200), CCR7 (3D12), CD95 (DX2), CD3 (SP34-2), and CD8 (SK1). After 15min in the dark, cells were washed and re-suspended in ice cold 1X PBS. Cells were sorted using a BD FACSAria II. Sorted $CD4^+$ T cells were FSC singlets, live, $CD45^+CD3^+CD4^+CD8^-$ lymphocytes and subsets were defined as follows: naïve ($CD95^-CD28^+CCR7^+$), central memory ($CD95^+CD28^+CCR7^+$), transitional memory ($CD95^+CD28^+CCR7^-$), and effector memory ($CD95^+CD28^-$). All antibodies are from BD Biosciences unless otherwise indicated. In study 1, sorted memory populations were pool into a single memory population and subject to proviral DNA analyses due to limiting cell numbers.

Virus sequencing. Virus sequencing of SIV recovered from plasma "blips" was performed essentially as described(*23*). Viral cDNA was diluted in 96-well plates to yield fewer than 30% wells positive for amplification to ensure that positive amplifications were a result of a single cDNA. Amplicons from cDNA dilutions resulting in less than 30% positive wells were sequenced at the Dana-Farber/Harvard Cancer Center DNA Resource Core. Raw cDNA sequence data was assembled using GeneCodes Sequencher 4.8 DNA sequencing software. All assembled sequence contigs were manually corrected for individual ambiguous nucleotide errors and further quality controlled to exclude any amplicons derived from multiple templates. Nucleotide alignments were made using the GeneCutter algorithm as described below (http://www.hiv.lanl.gov/content/sequence/GENE_CUTTER/cutter.html).

Viral phylogenetic analysis. The *gag* and *env* codon sequence alignments were manually reviewed after automatic alignment with Gene Cutter (hiv.lanl.gov/content/sequence/GENE_CUTTER/cutter.html).

Sequences were stratified by monkey and BioPerl (v1.006924) inferred a founder consensus sequence from plasma-derived variants sampled pre-treatment. A test for homogeneous infection, based on a null model of random sequence evolution in acute infection, compared the distribution of Hamming distances among sequences sampled from plasma before ART for a Poisson distribution(*36, 37*). The Hypermut utility (v2, hiv.lanl.gov/content/sequence/HYPERMUT/hypermut.html) identified sequences enriched for APOBEC-induced hypermutations relative to the founder reference sequence. For each animal, PhyML (v3) computed a phylogeny using the GTR nucleotide substitution model(*38*) and a four-category discrete approximation to a gamma distribution of evolutionary rates across sites, with an additional term for invariant sites(*39*). Parameters were inferred by maximum likelihood jointly with tree topology optimization with the resulting trees rooted on founder sequences. Newick Utilities (v1.6) summarized evolutionary distances to the founder sequence and omitted the sequences that exactly matched the founder by pruning from the tree. Trees were similarly pruned to show quasispecies development by cumulative stratification into groups sampled before, before/during, and before/during/after treatment. The R package ape rendered trees (v3.4).

***Ex vivo* virus outgrowth assay.** Peripheral blood mononuclear cells (PBMCs) were isolated using a ficoll-hypaque density gradient, then re-suspended at 2.0 x 10^6 cells/ml in RPMI 1640 media supplemented with 10% heat-inactivated fetal bovine serum, penicillin, streptomycin and 100nM raltegravir. PBMCs were then seeded into culture plates at 4 × 10^6 cells/well with or without and Con A stimulation. Cell cultures were then incubated at 37°C in a humidified 5% CO_2 atmosphere for 6 days. After 6 days in culture, cell-free supernatant was collected for the measurement of SIV RNA by qRT-PCR.

***In vitro* co-culture with CEMx174 cells.** CD8+ T cells were depleted from freshly-ficolled PBMC using Miltenyi's CD8 Microbead Kit for non-human primates according to manufacturer's instructions and quantified using the flow cytometry-based cell counter Guava EasyCyte (EMD Millipore). 5x10^6

CEMx174 cells were incubated at 37°C with $1x10^6$ CD8+ T cell-depleted PBMCs in 3 ml of culture media for 48 hrs. Culture media was added to up to 10 ml on day 3, and cells were split twice per week.

***In vivo* CD8+ T cell depletion.** RM were depleted of CD8+ lymphocytes (CD8+ T cells and NK cells) using the monoclonal antibody MT807R1 (Non-human Primate Reagent Resource) as previously described(*40*) using the following dosing schedule: on day 0, 10 mg/kg were delivered subcutaneously and on days 3, 7, and 10, 5 mg/kg were delivered intravenously. CD4 and CD8 lymphocytes were monitored twice weekly for the first three weeks and then weekly for the remaining monitoring period. Whole blood was stained with the antibodies CD4-PerCP-Cy5.5 (L200, BD Biosciences), CD8-PE (DK25, Dako), and CD3-APC (SP34.2, BD Biosciences). The anti-CD8 antibody clone DK25 has been previously determined to not be blocked by bound MT807R1 (*41*). Red blood cells were lysed using a TQ-prep (Beckman Coulter), fixed in 2% formaldehyde, acquired on a FACSCalibur (BD Bioscience), and analyzed using FlowJo Software. Complete blood counts (CBC) were analyzed on a Siemens ADVIA120. Frequencies of CD8 lymphocytes per volume blood were calculated using the percent CD8 lymphocytes, determined by flow cytometry, and the frequencies of total lymphocytes, determined by the CBC.

***In vivo* adoptive cell transfer.** For adoptive transfer experiments, fresh or frozen peripheral blood and lymph node mononuclear cells were utilized. For adoptive cell transfer prior to TLR7-agonist dosing, frozen PBMC and LMNC were used. For samples post therapy, fresh PBMC and LMNC were isolated from two remission RMs (at day 445 post ART stop). Cells were washed three times in PBS and then, infused into naïve rhesus monkeys by the intravenous (IV) route. Two RMs received either total 5.1 or 5.9×10^7 of cells infusions (prior to TLR7-agonist treatment) and the other two RMs received infusions of 12.7 or 12.3×10^7 cells (isolated on day 445 post ART stop).

Intracellular cytokine staining. Measurement IFN-γ on CD4+ and CD8+ T cells from fresh and cryopreserved PBMCs cells were performed as previously described[41]. Thawed PBMCs were rested at 37°C for 4hrs before stimulation. Approximately 3×10^6 cells were stimulated either with DMSO alone (unstimulated) or 2 μg/ml overlapping peptide pools covering the entire SIVmac239 Gag protein (NIH AIDS reagent Program, cat# 6204) and 1 μg/ml of anti-CD49d antibodies (BD Biosciences). The following conjugated antibodies and staining reagents were used for surface staining: CD4 (L200), CD95 (DX2), CD28 (L293), CD8 (SK1) and Yellow LIVE/DEAD Fixable Dead Cell Stain (Invitrogen). The following conjugated antibodies were used during intracellular staining: CD3 (SP34-2), IFN-γ (B27), and CD69 (TP1.55.3, Beckman Coulter). All antibodies are from BD Biosciences unless indicated otherwise. Value of percent IFN-γ-positive cells in unstimulated samples was subtracted from the corresponding value of stimulated samples(*42*).

Statistical analyses. Analyses of virologic or immunologic data at study entry were performed using Wilcoxon signed rank tests. Transformed log10 SIV RNA levels in plasma were calculated using GraphPad Prism (version 6.0). Comparisons of grouped variables and changes in values after treatment within groups were analyzed by use of a Wilcoxon signed rank test and a Wilcoxon matched-pairs signed rank test, respectively. P values were adjusted for multiple comparisons when more than two groups were compared. Changes in cytokines and chemokines levels in plasma after TLR7 treatment and its significance were displayed using a volcano plot. R package (Version 3.3.0) was used to generate heatmaps. Power calculations and 2-sample test for equality of proportions with continuity correction were conducted using G*Power (http://www.gpower.hhu.de) software.

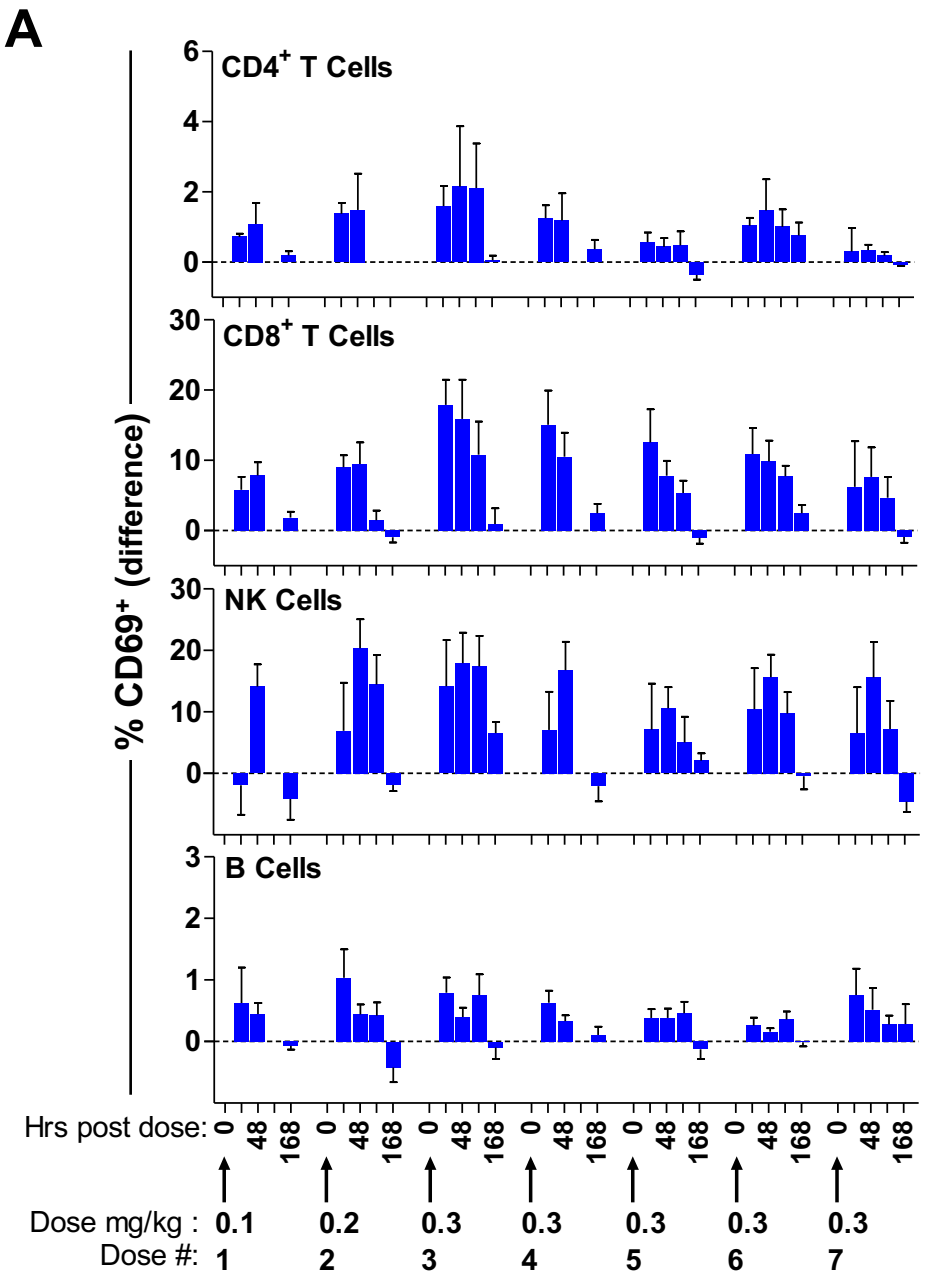
A
CD4+ T Cells
CD8+ T Cells
NK Cells
B Cells
% CD69+ (difference)
Hrs post dose: 0 48 168 0 48 168 0 48 168 0 48 168 0 48 168 0 48 168 0 48 168
Dose mg/kg : 0.1 0.2 0.3 0.3 0.3 0.3 0.3
Dose #: 1 2 3 4 5 6 7

Figure 1A

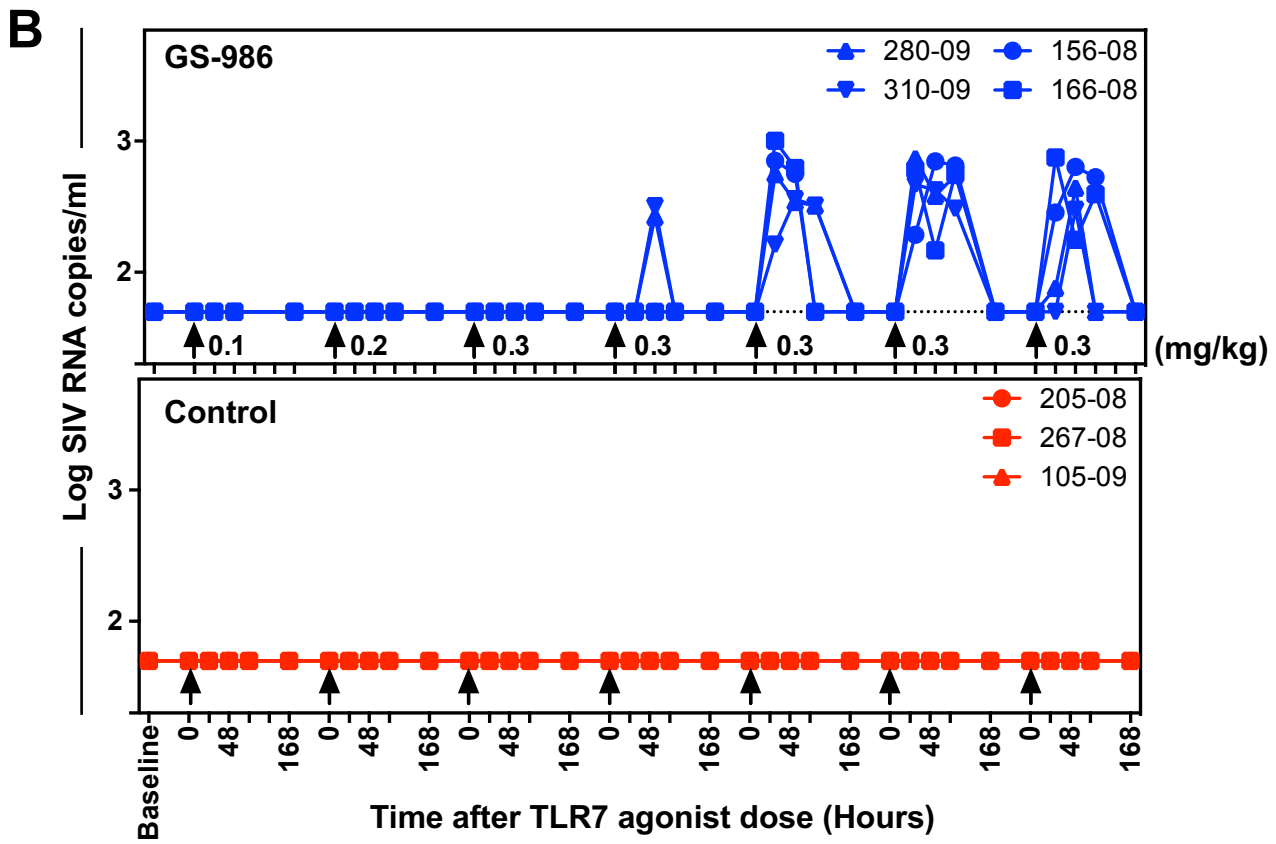
B
GS-986
280-09
156-08
310-09
166-08
Log SIV RNA copies/ml
3
2
0.1
0.2
0.3
0.3
0.3
0.3
0.3
(mg/kg)
Control
205-08
267-08
105-09
3
2
Baseline
0
48
168
Time after TLR7 agonist dose (Hours)

Figure 1B

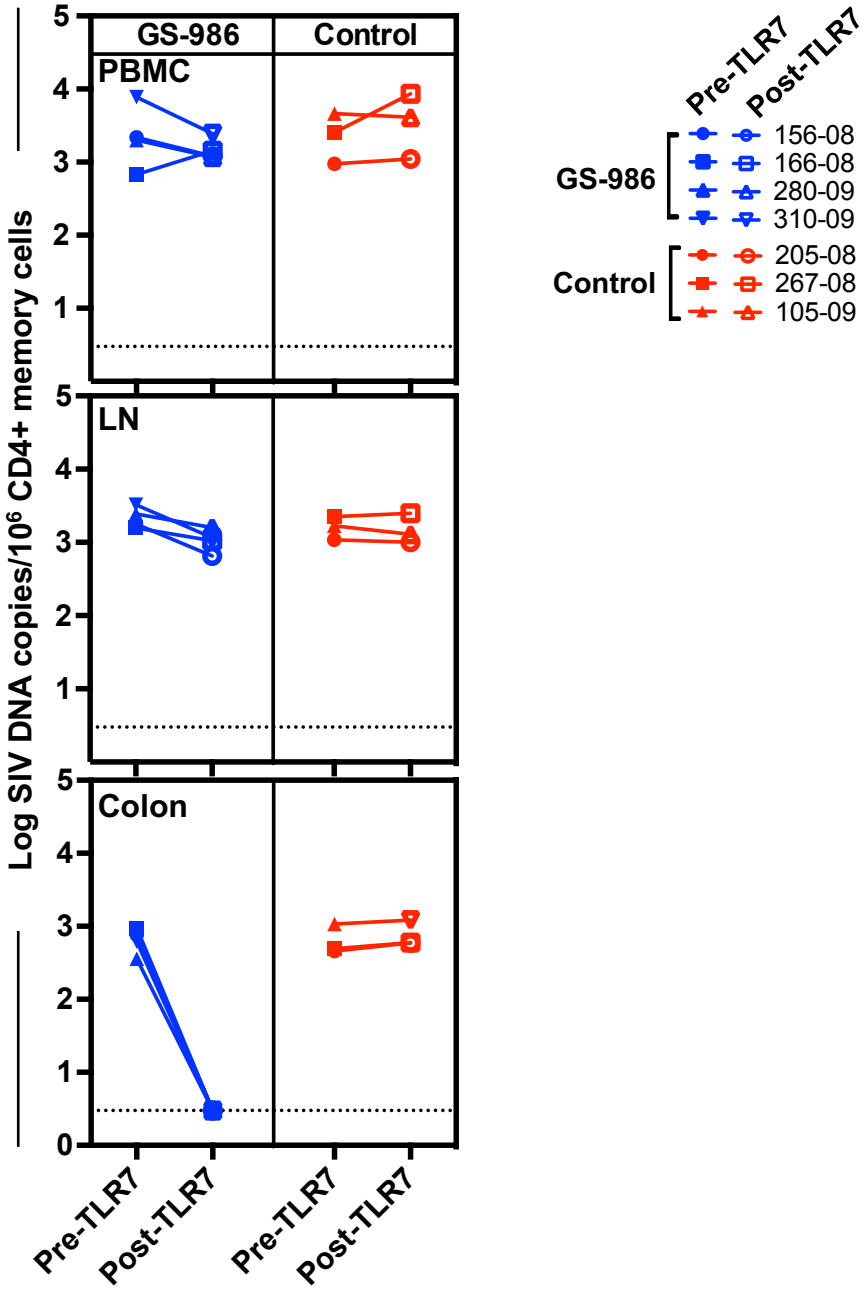
GS-986
Control
PBMC
LN
Colon
Log SIV DNA copies/10^6 CD4+ memory cells
0
1
2
3
4
5
Pre-TLR7
Post-TLR7
Pre-TLR7
Post-TLR7
Pre-TLR7
Post-TLR7
GS-986
156-08
166-08
280-09
310-09
Control
205-08
267-08
105-09

Figure 2

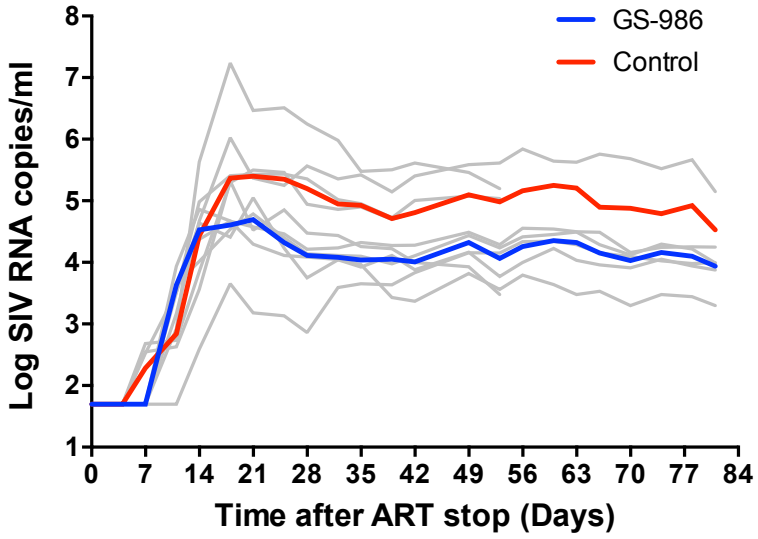
GS-986
Control
Log SIV RNA copies/ml
8
7
6
5
4
3
2
1
0
7
14
21
28
35
42
49
56
63
70
77
84
Time after ART stop (Days)

Figure 3

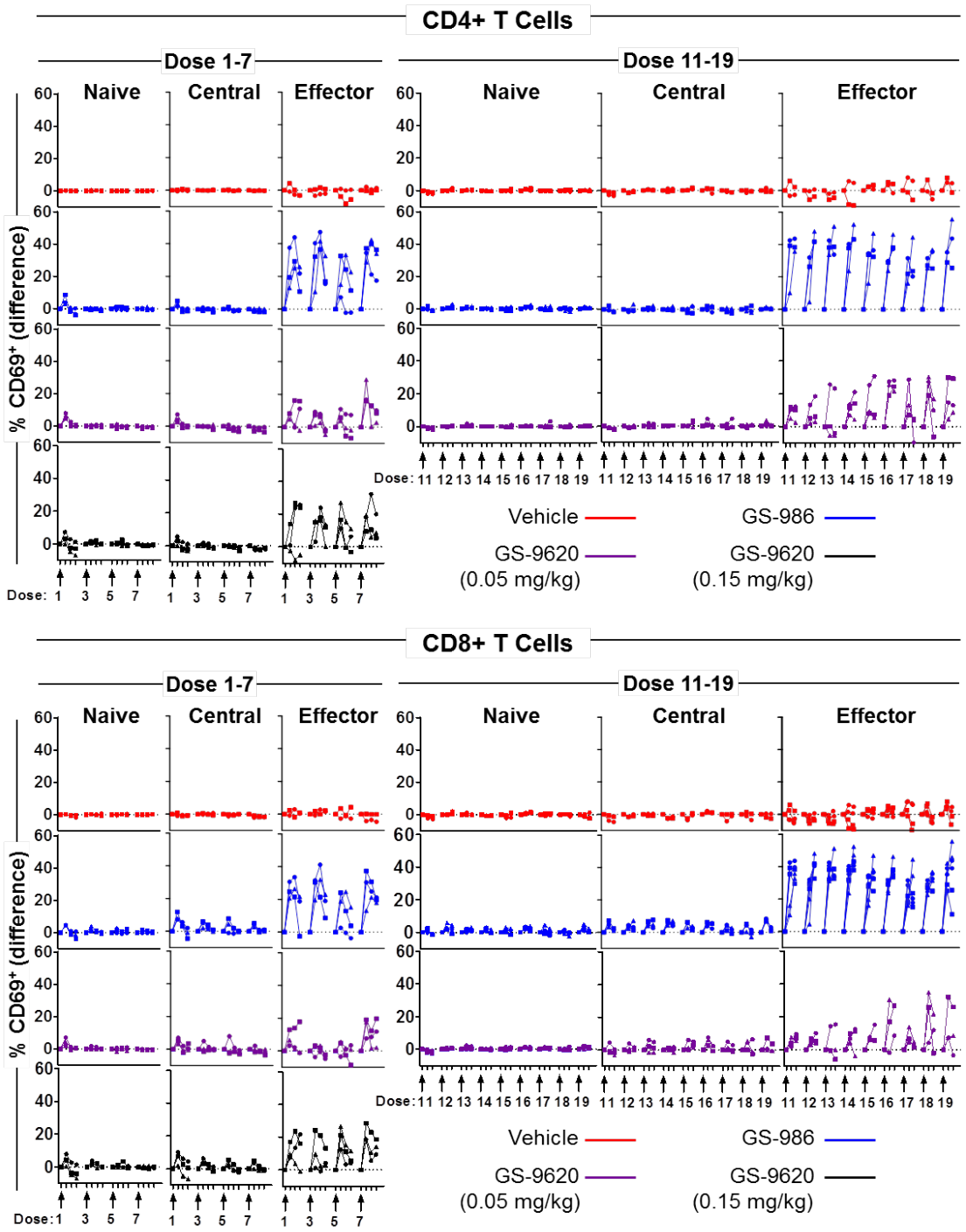
A
CD4+ T Cells
Dose 1-7
Dose 11-19
Naive
Central
Effector
% CD69+ (difference)
Dose: 1 3 5 7
Dose: 11 12 13 14 15 16 17 18 19
Vehicle
GS-986
GS-9620 (0.05 mg/kg)
GS-9620 (0.15 mg/kg)
B
CD8+ T Cells
Dose 1-7
Dose 11-19
Naive
Central
Effector
% CD69+ (difference)
Dose: 1 3 5 7
Dose: 11 12 13 14 15 16 17 18 19
Vehicle
GS-986
GS-9620 (0.05 mg/kg)
GS-9620 (0.15 mg/kg)

Figure 4

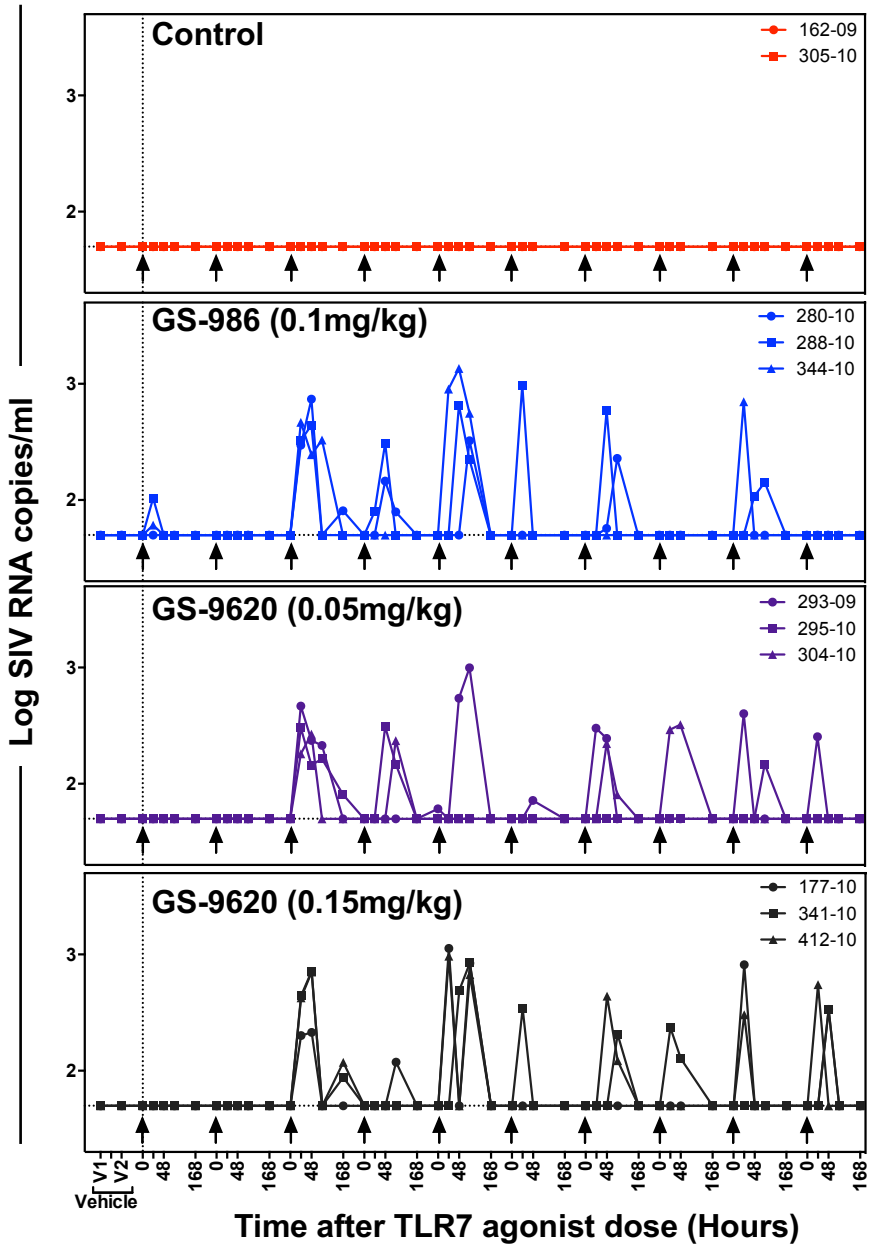
Control
162-09
305-10
GS-986 (0.1mg/kg)
280-10
288-10
344-10
GS-9620 (0.05mg/kg)
293-09
295-10
304-10
GS-9620 (0.15mg/kg)
177-10
341-10
412-10
Log SIV RNA copies/ml
3
2
V1
V2
Vehicle
0
48
168
Time after TLR7 agonist dose (Hours)

Figure 5

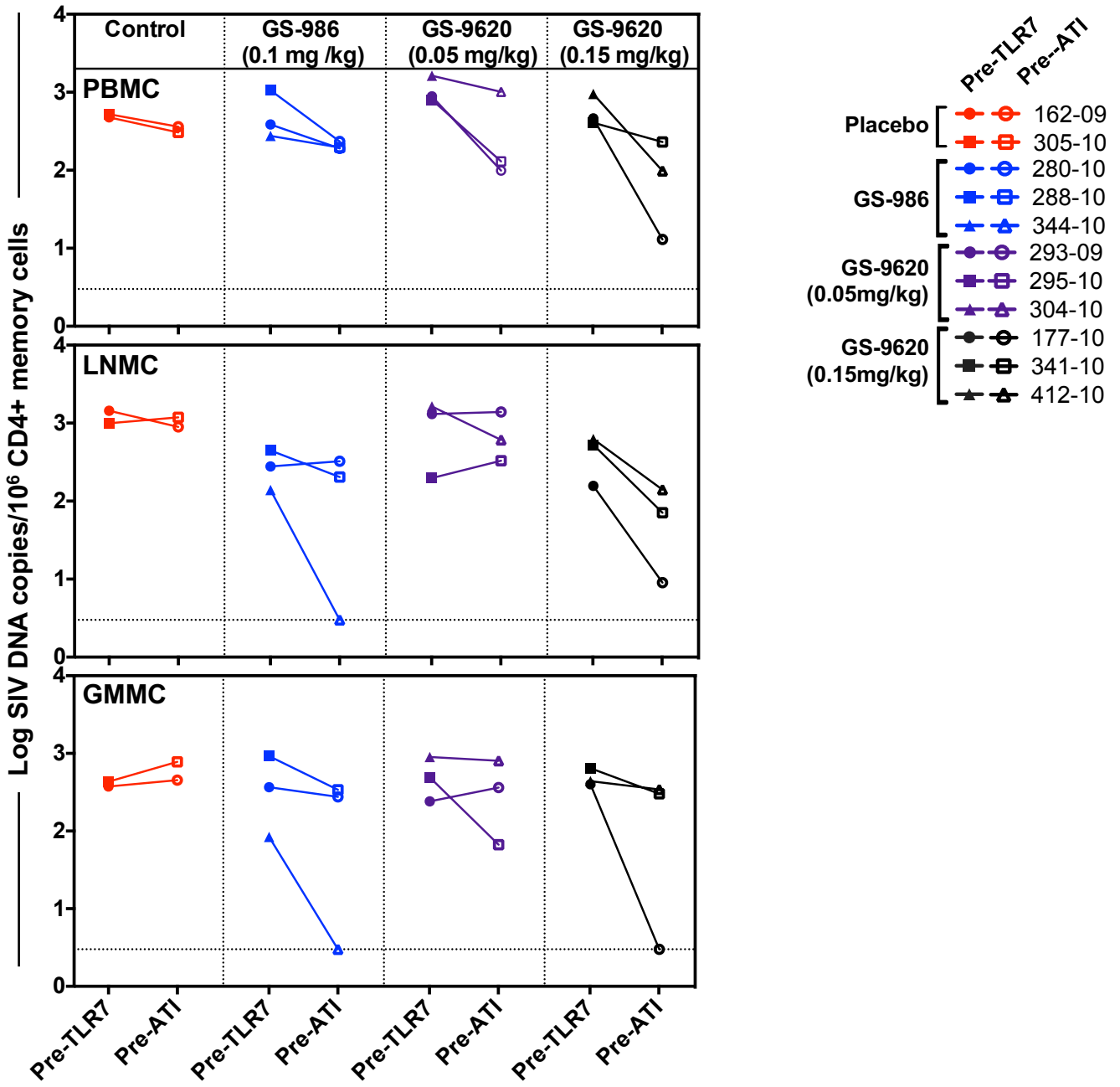
Control
GS-986 (0.1 mg /kg)
GS-9620 (0.05 mg/kg)
GS-9620 (0.15 mg/kg)
PBMC
LNMC
GMMC
Log SIV DNA copies/10^6 CD4+ memory cells
0
1
2
3
4
Pre-TLR7
Pre-ATI
Pre-TLR7
Pre-ATI
Pre-TLR7
Pre-ATI
Pre-TLR7
Pre-ATI
Pre-TLR7
Pre--ATI
Placebo
162-09
305-10
GS-986
280-10
288-10
344-10
GS-9620 (0.05mg/kg)
293-09
295-10
304-10
GS-9620 (0.15mg/kg)
177-10
341-10
412-10

Figure 6A

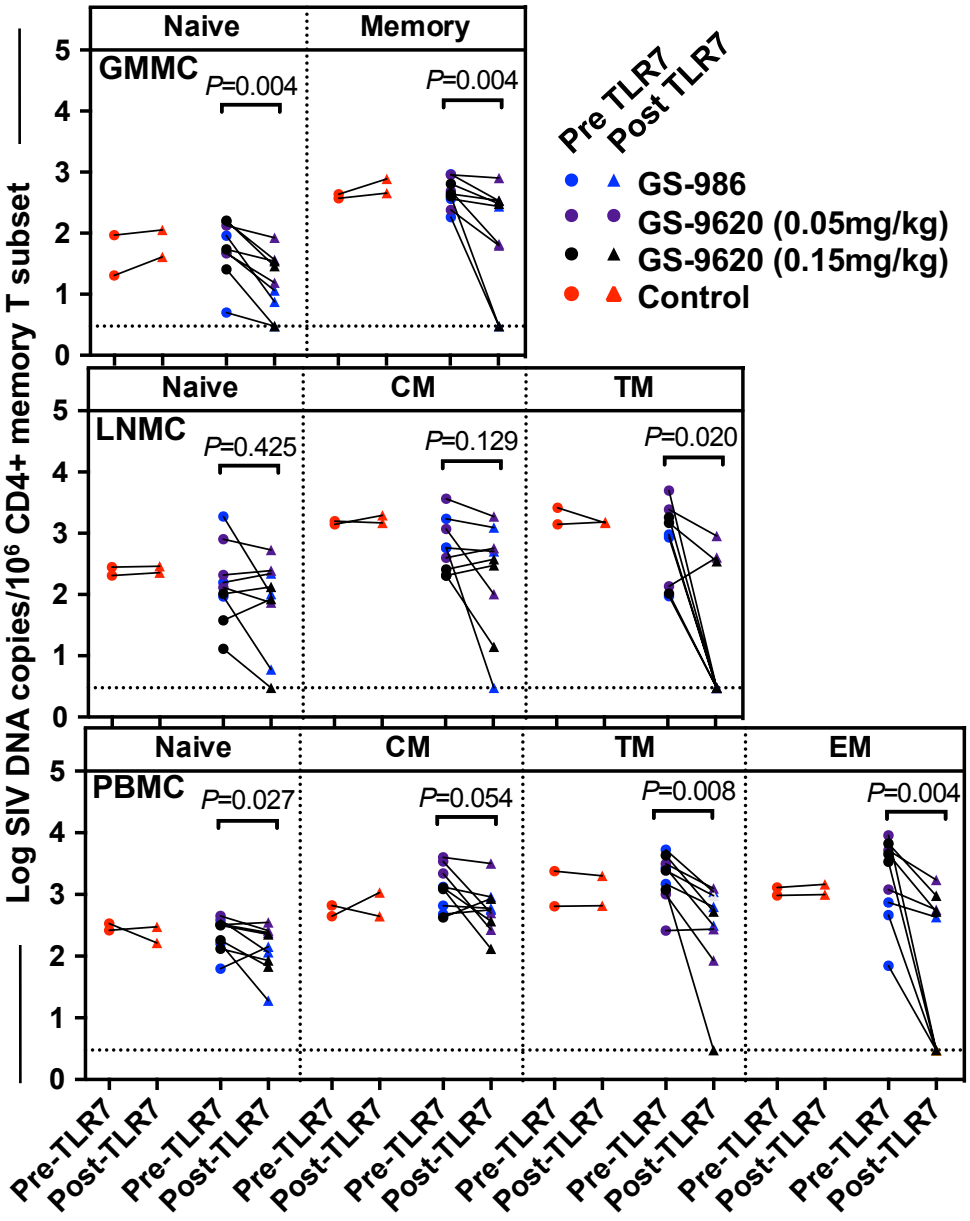
Naive
Memory
GMMC
P=0.004
P=0.004
Pre TLR7
Post TLR7
GS-986
GS-9620 (0.05mg/kg)
GS-9620 (0.15mg/kg)
Control
Naive
CM
TM
LNMC
P=0.425
P=0.129
P=0.020
Naive
CM
TM
EM
PBMC
P=0.027
P=0.054
P=0.008
P=0.004
Log SIV DNA copies/10^6 CD4+ memory T subset
0
1
2
3
4
5
Pre-TLR7
Post-TLR7

Figure 6B

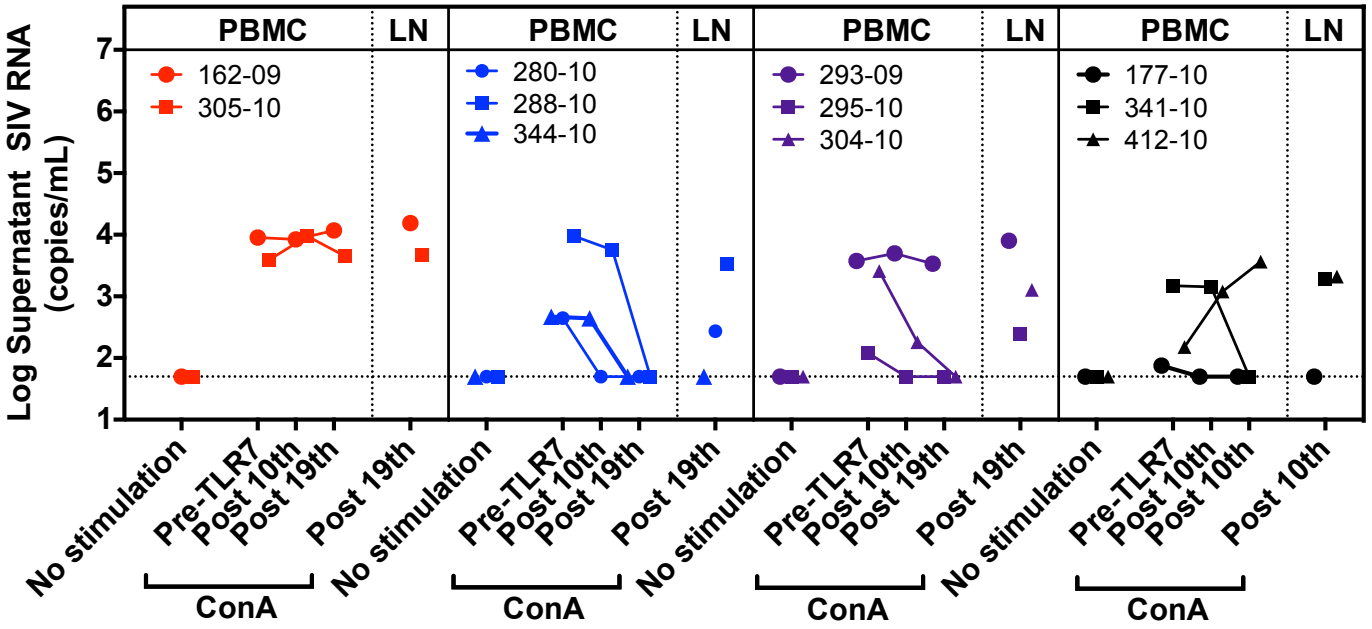
Log Supernatant SIV RNA (copies/mL)
7
6
5
4
3
2
1
PBMC
LN
PBMC
LN
PBMC
LN
PBMC
LN
162-09
305-10
280-10
288-10
344-10
293-09
295-10
304-10
177-10
341-10
412-10
No stimulation
Pre-TLR7
Post 10th
Post 19th
Post 19th
No stimulation
Pre-TLR7
Post 10th
Post 19th
Post 19th
No stimulation
Pre-TLR7
Post 10th
Post 19th
Post 19th
No stimulation
Pre-TLR7
Post 10th
Post 10th
Post 10th
ConA
ConA
ConA
ConA

Figure 6C

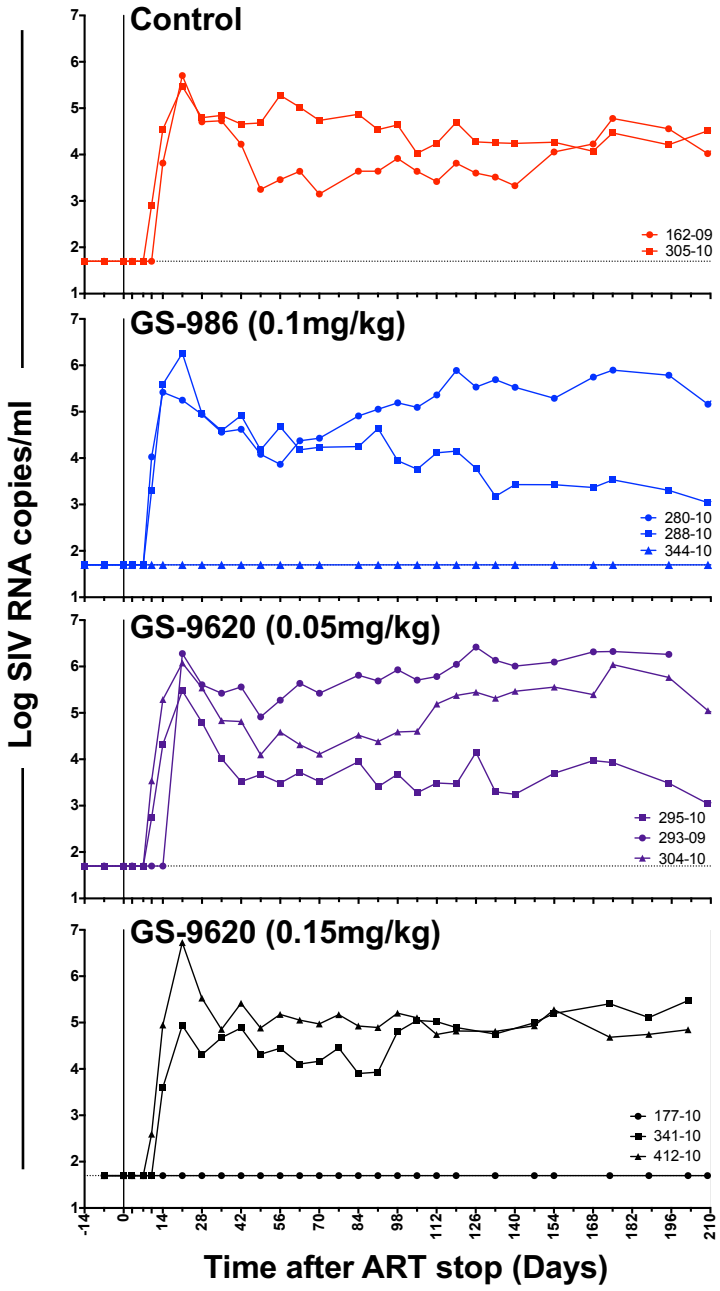
Control
GS-986 (0.1mg/kg)
GS-9620 (0.05mg/kg)
GS-9620 (0.15mg/kg)
Log SIV RNA copies/ml
Time after ART stop (Days)
162-09
305-10
280-10
288-10
344-10
295-10
293-09
304-10
177-10
341-10
412-10

Figure 6D

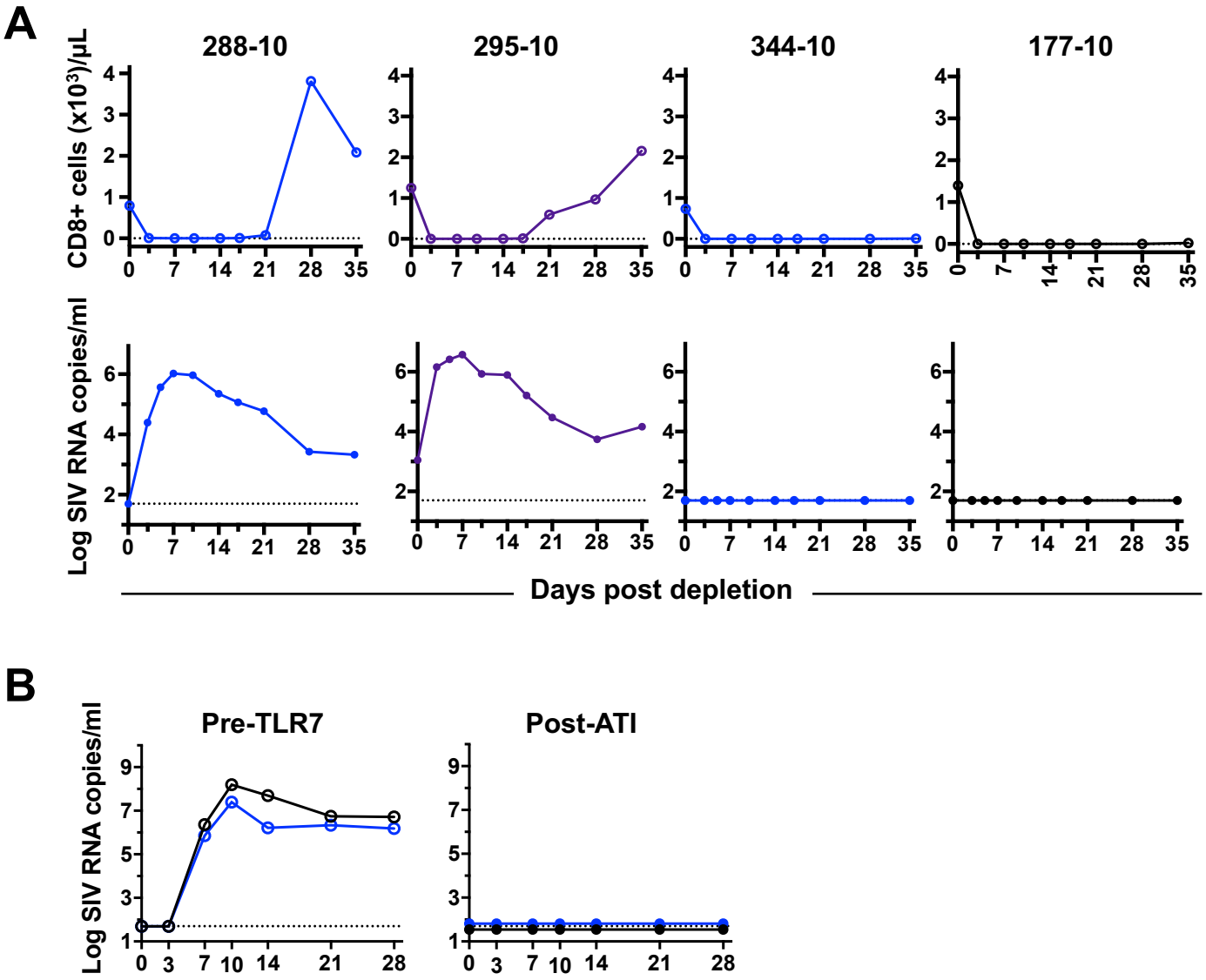
A
288-10
295-10
344-10
177-10
CD8+ cells (x10³)/µL
Log SIV RNA copies/ml
Days post depletion
B
Pre-TLR7
Post-ATI
Log SIV RNA copies/ml

Figure 7A-B

TLR7 Agonists Induce Transient Viremia and Reduce the Viral Reservoir in SIV-Infected Monkeys on Antiretroviral Therapy

So-Yon Lim[1], Christa E. Osuna[1], Joe Hesselgesser[2], Peter T. Hraber[3] Jeffrey M. Gerold[4], Tiffany L. Barnes[2], Srisowmya Sanisetty[1], Michael S. Seaman[1], Mark G. Lewis[5], Romas Gelezunias[2], Michael D. Miller[2], Tomas Cihlar[2], William A. Lee[2], Alison L. Hill[4] and James B. Whitney[1,6*]

[1]Center for Virology and Vaccine Research, Beth Israel Deaconess Medical Center, Harvard Medical School, Boston, MA 02215, USA; [2]Gilead Sciences Inc., Foster City, CA 94404; [3]Los Alamos National Laboratory, Los Alamos, NM 87545; [4]Program for Evolutionary Dynamics, Harvard University, Cambridge, MA 02138 USA; [5]Bioqual, Rockville, MD 20852, USA; [6]Ragon Institute of MGH, MIT, and Harvard, Cambridge, MA 02139, USA

*Corresponding author

Supplemental Methods

Viral dynamics modeling. We used viral dynamics models for three different purposes in the study: i) to characterize the kinetics of viral rebound after ART cessation among animals who rebounded, ii) to estimate the number of latent cells that would have needed to be reactivated to explain the blip dynamics seen during TLR7-agonist + ART therapy, and iii) to estimate the latent reservoir reduction that would be needed to explain the lack of rebound in treated animals who did not rebound after ART cessation.

i) Modeling rebound kinetics after ART cessation: We fit each viral load time course to a standard model of viral dynamics [1] that describes the changes over time in levels of uninfected and infected target cells of the virus, along with free virus, using a system of ordinary differential equations (**figure S15A**):

$$\dot{T} = \lambda - \beta TV - d_T T$$

$$\dot{I} = a + \beta TV - d_I I$$

$$\dot{V} = kI - cV$$

where T is the concentration of uninfected target $CD4^+$ T cells (cell/uL), I is the concentration of infected $CD4^+$ T cells (cell/mL), V is the viral load (copies/mL), λ is the rate of production of susceptible uninfected cells (cells/uL/day), β is the viral infectivitiy ($(copies/mL)^{-1}$ day^{-1}), d_I is the death rate of infected cells (day^{-1}), d_T is the death rate of death of uninfected cells (day^{-1}), a is the rate at which latent cells reactivate to become productively infected [2–5], k is the viral burst size (virions/cell)(day^{-1}) and c is the viral clearance rate (day^{-1}) .

Because free virus is produced and cleared rapidly, levels are expected to equilibrate very rapidly with respect to infected cell levels, and we employed the common assumption that these two quantities are proportional. Consequently, the model reduces to:

$$\dot{T} = \lambda - \beta TV - d_T T$$

$$\dot{V} = a\left(\frac{k}{c}\right) + \beta T\left(\frac{k}{c}\right)V - d_I V$$

During ART, $\beta = 0$, and x and v reach a steady state at values $T_0 = \lambda/d_T$ and $V_0 = (a/d_I)(k/c)$, which we take as the initial conditions at the time of ART interruption.

Note that this model assumes that some virus is present (due to stable release from reservoirs) immediately upon ART cessation and infection begins immediately. The reservoir exit rate a, and hence the initial value V_0 is expected to be related to both the size and the activation rate of the functional viral reservoir. If the reservoir is so small, or so infrequently reactivating, that there is a delay between ART interruption and the start of the infection growth, this can be captured with very low a values. Separately, we used a stochastic model of functional reservoir activation to understand why some animals have not rebounded (see iii).

The model was fit to longitudinal values of logarithmic plasma viral load (**figure S15B**). Because direct measurements were not available for target cell levels (a subset of the total CD4 T cell population), the parameter λ and the combination (k/c) are not simultaneously identifiable. Accordingly, the ratio (k/c) was fixed to 2000 virus/cell based on a burst size of $k = 5\times10^4$ (virions/cell)(day^{-1}) and c=23 day^{-1} for SIV [6–8]. In total, five parameters were fit $(\lambda, \beta, a, d_T, d_I)$. The inference procedure was formulated in a likelihood framework which treats data below the viral load detection threshold of 50 copies/mL as censored. We assumed the observed viral load is log-normally distributed around the true viral load, which added an extra parameter for the measurement error variance σ^2. We maximized the likelihood over a log-transformed parameter space constrained by physiologically reasonable bounds: $log10(\lambda) \in [-2, 3]$, $log10(\beta) \in [-10,0]$, $log10(a) \in [-18\ -2]$, $log10(d_T) \in [-4, 2]$, $log10\left(\frac{d_I}{d_T}\right) \in [0, 3]$. The differential equations were numerically integrated for each parameter value using *ode45* and fits were obtained using the *fminsearchbnd*, both in MATLAB R2015a (http://www.mathworks.com/matlabcentral/fileexchange/8277-fminsearchbnd--fminsearchcon).

For each animal, we started the fitting procedure using at least 10 random initial condition values and chose the best resulting fit.

After fitting each model, we derived two composite parameters from model parameters – the exponential growth rate of the virus immediately following rebound r, and the predicted set-point viral load, V_{SP} (**figure S13C-F**, **Table S1**) In the realistic scenario where *a* is small and the residual viremia during ART is much less than viral loads off ART, these quantities are related to the model parameters by the following equations:

$$r = \frac{\lambda\beta}{d_T}\left(\frac{k}{c}\right) - d_I$$

$$V_{SP} = \frac{\lambda}{d_I}\left(\frac{k}{c}\right) - \frac{d_T}{\beta}$$

In order to estimate how uncertainty in measurements of viral load data propagate to uncertainty in parameter estimates, we performed a perturbation analysis of our fitting procedure. Using the average error from our unperturbed fits of viral load in each animal on a logarithmic scale, we added noise to the viral load data above the detection limit by sampling from a normal distribution with matched variance and re-fit model parameters many times. All fits were visually inspected to ensure the minimization routine was not obviously caught in a local optimum. We performed statistical tests between treatment and control groups in order to ascertain statistically significant differences, which included parameter estimate uncertainties. All tests were performed using unpaired, two-sided, Welch's unequal variances *t*-tests [9]. The total sample variance for each group, s^2, was calculated as $s^2 = m^2 + \sum_j p_j^2 /N$, where m^2 is the sample variance of the best estimated parameter values, and p_j^2 is the perturbation variance for each individual.

Comparing parameters between pooled controls and pooled treated animals from both phases, we found that reactivation was lower in treated animals vs controls (mean $\log_{10}(a)$ -9.87 vs -5.65 cell/ml/day, p=0.01), while viral growth rate was higher in treated animals vs controls (mean $\log_{10}(r)$ 0.25 vs -0.11 /day, corresponding to *r* of 1.80 vs 0.77/day, p=0.03). There was no

significant difference in predicted set-point viral load or time to rebound. Comparing pooled controls to only those treated in Phase 1, the same trends held: in treated vs control animals, mean $\log_{10}(a)$ -10.17 vs -5.65 cell/ml/day (p=0.03) and mean $\log_{10}(r)$ -0.31 vs -0.11 /day (p=0.02). For Phase 2, pooling all controls, mean $\log_{10}(a)$ -9.71 vs -5.65 cell/ml/day (p=0.05) and mean $\log_{10}(r)$ 0.22 vs -0.11 /day (p=0.05). No significant differences were found in the other basic model parameters for either phase ($p > 0.4$), except in Phase 1, where the viral infectivity β, was significantly increased in treated animals ($p = 0.001$). We repeated all statistical tests with Phase 1 control animal 205-08, as this animal fit least well with the model, and had very slow growth of viral load towards a set point without first reaching a peak. All the above trends were robust to removal of this outlier. We also repeated the model fitting assuming a "washout period" during which antiretroviral drugs were still decaying and the virus could not spread. Increasing this washout period to 1 or 3 days increased the estimated values of reactivation rate (a) but did not change the results of comparisons between groups.

ii) Modeling reservoir reactivation during TLR7-agonist administration: To estimate the amount of latent cell reactivation needed to explain the observed blips, we used a similar model as above (**figure S15A**), but assumed that $\beta = 0$ during ART administration, and that the administration of the TLR7-agonist caused the reactivation rate a to change to an amount $a + a_{LRA}$. We assumed that a_{LRA} was a constant, starting from a time t_0 after TRL7-agonist dosing began and continuing for a time τ. We allowed a_{LRA} to vary between each animal and each dose. We used the same fitting procedure described in (i), except that an analytic formula for $V(t)$ could be derived. We compared two scenarios for what happens when TLR7-agonist action stops – either reactivation ceases ($a_{LRA} \rightarrow 0$) but cells that are already reactivated continue to produce virions, or, virion production in reactivated cells also ceases. We found that the later scenario fit the blip data much better (**figure S15B**). For this model, the equations for viral load are:

$$V(t) = \begin{cases} \left(\frac{k}{c}\right)\left(\frac{a}{d_I}\right) & t < t_0 \\ V(t_0) + \left(\frac{k}{c}\right)\left(\frac{a_{LRA}}{d_I}\right)\left(1 - \left(\frac{ce^{-d_T(t-t_0)} - d_I e^{-c(t-t_0)}}{c - d_I}\right)\right) & t_0 < t < \tau \\ V(t_0) + V(\tau)e^{-ct} & t > \tau \end{cases}$$

In all cases we fixed $k = 5{\times}10^4$ (virions/cell) (day^{-1}) and c=23 day^{-1} for SIV as above. To estimate d_I for each animal, we fit the decay rate of viral load once ART was initiated to a simple exponential function (**figure S16**). We used a=10^{-3} cell/ml/day which was the maximum value estimated above during rebound, though using alternate values of a that result in viral load below the detection limit before TLR7-agonist dosing do not influence the results. Results depend to some extent on the values of d_I, k, and c. If TLR7-agonist-induced latent cells produce less virus over their lifespan than actively infected cells (e.g. due to incomplete activation), then the observed blips correspond to even higher numbers of actively infected cells. If they produce more virus (e.g. by avoiding immune detection), then blips could be explained with less reactivation.

For each animal, the total reactivated cells over the entire treatment period was calculated as $\sum_{i=1}^{n\_doses} a_{ART,i}\ \tau_i$. In all TLR7-agonist treated animals we found that between 1-4 cells/ml were likely activated which corresponds to 0.1-1% of SIV DNA+ PBMCs. (Supplemental Table 2). Because other work has shown that for HIV only a few percent of DNA+ cells contain inducible or replication-competent virus [10,11], it is plausible that a large fraction of the reservoir could have been reduced with these blip sizes.

iii) Modeling delay in viral rebound due to reservoir reduction. For animals who did not experience rebound, we were interested in how much the reservoir would need be have been reduced by the treatment to explain the long delay in rebound, assuming that this was the only mechanism for control. We used a previously developed stochastic model for HIV rebound dynamics [3] and adjusted the parameter values to represent the dynamics in SIV-infected

macaques. Specifically, we reduced the total number of latently-infected cells before intervention by 10-fold, representing the approximate weight difference between macaques and humans, while keeping the infected frequency the same (~ 1 IUPM). We increased the viral growth rate to r = 0.8 since viral loads grow more rapidly post-rebound in these animals (**Table S1**, **figure S15D**, [3]) compared to humans (who have r ~ 0.4), and we adjusted the number of cells reactivating from the reservoir each day to ~25 (compared to ~60 in humans) so that the average rebound time (to 50 copies/ml) was around 8 days assuming three days for drug washout (**Table S1**, **figure S15F,** [12]). We kept the parameter determining the noise in viral burst size the same and also assumed the death rate of latently infected cells was the same as in humans [3]. In keeping with our findings here and elsewhere [13], we assume that there may be inter-individual variation in these parameters. In particular, we allowed the growth rate and reactivation rate to be log-normally distributed with log-means at the values given above, and log-standard deviations of 0.5 and 0.2 respectively.

With these values, we ran the model to determine the distribution of expected rebound times (or probability of cure) as a function of the reduction in the reservoir conferred by treatment (**figure S13G**). These results demonstrate that observable delays in rebound time are not expected unless there are large reductions in the size of the intact reservoir. Even robust reductions up to 10-fold in all animals may not be observable in rebound times unless cohorts are very large. Consequently, the observation of rebound in most TLR7-agonist-treated animals does not rule out a modest but incomplete effect of the drug on the reservoir size.

We next used a previously-developed Bayesian approach [14] to determine which reservoir reductions were most likely given the joint observations of a particular time off treatment (2 years) and a negative co-culture assay (using 4 million cells) [15] (**figure S15H**). We found that a 1,400-fold reduction in the reservoir is most likely given these findings (95% CI [110, 32 000]).

Note that this model ignores the fact that improved immune function due to TLR7-agonist treatment may also contribute to the control observed in two animals, and therefore the reservoir reductions estimates only apply in the case that this is the sole mechanism for rebound delay. Given that CD8+ T cell depletion did not lead to loss of control in these animals, we believe this is a reasonable hypothesis.

Table S1. Parameters derived from viral dynamics models. Estimates and uncertainties for a, the rate of exit of actively infected cells from the latent reservoir; r, the exponential growth rate of virus immediately following rebound initiation; and V_{SP}, the predicted eventual set-point viral load. Rebound time is the predicted time at which viral load crossed the rebound threshold of 50 copies/mL. "Best" values are the best-estimated parameter fits using the measured data. "STD" values are the standard deviation of parameter values returned from the perturbation analysis. Parameter estimation and perturbation procedures are described in the Supplementary Methods.

			$\log_{10}(a)$ (c/mL)		**$\log_{10}(r)$ (day^{-1})**		**$\log_{10}(V_{SP})$ (c/mL)**		**Rebound time (days)**
Phase	**Dose**	**ID**	**Best**	**STD**	**Best**	**STD**	**Best**	**STD**	**Best**
1	Placebo	205-08	-2.94	6.20	-0.81	0.39	4.12	0.16	6.3
		267-08	-3.78	0.58	-0.20	0.03	4.98	0.50	5.8
		105-09	-6.21	0.94	0.06	0.30	5.52	0.05	8.5
		234-09	-8.48	0.70	0.19	0.35	5.10	0.75	9.1
		322-09	-4.32	0.53	-0.20	0.03	3.63	0.31	6.3
		374-09	-4.67	0.13	-0.08	0.02	2.72	0.18	5.7
1	GS-986 (0.1, 0.2, 5*0.3) mg/kg	156-08	-7.79	2.52	0.07	0.14	3.79	0.17	11.6
		166-08	-7.01	0.96	0.05	0.21	3.37	0.52	10.6
		280-09	-10.08	2.92	0.31	0.17	3.57	0.12	8.4
		310-09	-11.16	2.44	0.34	0.03	3.90	0.11	9.0
2	Placebo	162-09	-10.23	1.99	0.36	0.06	4.29	0.06	8.9
		305-10	-9.20	2.33	0.23	0.10	4.36	0.30	8.3
2	GS-986, 0.1mg/kg	280-10	-10.06	1.91	0.37	0.03	4.73	0.17	8.4
		288-10	-11.18	2.79	0.37	0.04	4.25	0.14	9.3
		344-10	-	-	-	-	-	-	-
	GS-9620, 0.05 mg/kg	293-09	-14.77	1.72	0.30	0.05	5.59	0.05	15.3
		295-10	-6.27	1.46	0.03	0.03	3.68	0.37	9.6
		304-10	-6.48	1.90	0.12	0.06	4.77	0.12	8.3
	GS-9620, 0.15 mg/kg	177-10	-	-	-	-	-	-	-
		341-10	-12.12	1.81	0.25	0.02	2.87	0.25	13.3
		412-10	-7.06	1.54	0.12	0.16	5.16	0.44	9.4

Table S2. Estimated number of latent cells reactivated during TLR7-agonist dosing period. A mathematical model of latent cell reactivation and virion production and clearance was fit to the viral load blips observed during the entire course of TLR7-agonist treatment for both study Phases. Results of the model fit were used to estimate the total number of reactivated cells over all doses (Supplementary Methods). CD4 counts and SIV DNA levels in PBMC were measured immediately prior to TLR7-agonist dosing.

Phase	Dose	ID	Required SIV^+ cells reactivated in plasma to explain blip size [cell/ul]	SIV DNA^+ cells / 10^6 $CD4^+$ T cells	CD4 count [cells/ul]	% of all SIV^+ $CD4^+$ T cells reactivated to explain blip size [%]
1	GS-986 (0.1, 0.2, 5*0.3) mg/kg	156-08	0.0027	816	668.3	0.5%
		166-08	0.0032	327	825.93	1.2%
		280-09	0.0024	973	905.58	0.3%
		310-09	0.0015	2280	745.29	0.1%
2	GS-986, 0.1mg/kg	280-10	0.0036	387	1443.16	0.6%
		288-10	0.0026	1058	352.8	0.7%
		344-10	0.003	276	1202.18	0.9%
	GS-9620, 0.05 mg/kg	293-09	0.0033	887	620.1	0.6%
		295-10	0.0012	801	1001.07	0.1%
		304-10	0.0014	1627	1160.64	0.1%
	GS-9620, 0.15 mg/kg	177-10	0.0023	463	1162.7	0.4%
		341-10	0.0028	407	703.12	1.0%
		412-10	0.002	950	821.49	0.3%

Supplementary Figures

Figure S1. **Effective suppression of SIV replication after ART and study randomization.** Log plasma virus RNA was monitored in RMs from the day of SIVmac251 infection to the initiation of TLR7 agonist therapy **(A)**. The initial viral burden and days to the complete viral suppression from the initiation of ART between groups of animals treated with TLR7 agonists or control were compared **(B)**. Open and solid circles represent animals used in the Study 1-(TLR7-treated, ○; Control, ○) and Study 2-(TLR7-treated, ●; Control, ●) respectively. Plots show the median with interquartile range. The comparison of the values between groups was determined using a Mann-Whitney test.

Figure S2. Study schema of TLR7 agonist dosing. In Study 1, 4 ART-suppressed monkeys received 7 doses of GS-986: 1 dose at 0.1 mg.kg, 1 at 0.2 mg/kg, and then 5 at 0.3 mg/kg. 6 control monkeys received formulation vehicle only **(A)**. Doses were administered every other week (EOW). ART was discontinued 2 weeks after the last TLR7 agonist dose. In Study 2, 11 monkeys were distributed into 4 groups: 2 in placebo (vehicle only), 3 in GS-986 at 0.1 mg/kg, 3 in GS-9620 at 0.05 mg/kg, and 3 in GS-9620 at 0.15 mg/kg **(B)**. 10 doses were administered EOW followed by a 3-month period without dosing after which monkeys in the placebo, GS-986 0.1 mg/kg, and GS-9620 0.05 mg/kg groups resumed dosing for 9 additional doses, again EOW. 2 weeks after the last dose, ART was discontinued in all 4 groups.

Figure S3. Induction of IFN-α by TLR7 agonist dosing. Dose-dependent induction of plasma IFN-α in RMs treated with escalating doses of GS-986 (Study 1) **(A)**. Dose-dependent induction of IFN-α in RMs treated with GS-986 or GS-9620 (Study 2) **(B)**. The dose concentrations of GS-986 or GS-9620 are indicated. Shaded areas represent 24-hour post-dosing of TLR7 agonist.

Figure S4A. Cumulative *gag* and *env* phylogenies from GS-986 treated RMs. Cumulative phylogenies from four treated RMs: 156-08, 166-08, 310-09, and 280-09. For clarity, sequences that exactly matched the T/F sequence are excluded. Symbol shapes indicate the compartment from which the sequence was sampled: PL, cell-free plasma RNA; PB, cell-associated proviral DNA from peripheral blood mononuclear cells (PBMCs); CR, proviral colorectal DNA; and LN, proviral lymph node DNA. Sequences sampled pre-treatment appear in the left-hand column. The middle column additionally shows plasma and PBMC sequences sampled during viremic blips. The right column adds post-treatment sequences to the previous two. Symbol fill colors indicate when the sequence was sampled, whether solid (pre-GS-986 treatment), intermediate grey or red (viremic blip), or open (post-treatment). Hypermutated sequences ($p<0.05$ by Hypermut v2) are indicated by red symbols. Maximum-likelihood trees were obtained with phyml and GTR with gamma-four rate heterogeneity. Trees were rooted on the transmitted-founder sequence, taken as the consensus among pre-treatment sequences, then ladderized. For each RM, the scale is kept the same.

Figure S4B. Cumulative *gag* and *env* distributions of genetic distances from the founder sequences in TLR7 agonist (GS-986) treated RMs. Sequences that exactly matched the SIV founder sequence were excluded, for clarity. This representation follows **Figure S4A** in layout and symbol representation. Rather than phylogenies, sequences are stratified by anatomical tissue. Sequences from pre-treatment (left column), then with added sequences from blip viremia (middle column), then post-treatment (right column), are included cumulatively. Symbol fill indicates sample timing. Superimposed lines indicate the quartiles (25 percentile, median, and 75 percentile) of each distribution. The x-axis uses a nonlinear (square-root transformed) scale to compare small distances.

Figure S5. *env*-Pseudovirus neutralization assay. Panels of 11 Env-pseudoviruses were produced to characterize the spectrum of their infectivity using a TZM-bl assay. SIV *env* sequences that were chosen to be cloned are isolates from SIV RNA blips (n=4) (**A)** or hypermutated viral DNA (n=7) (**B**). Infectivity is expressed as relative light units (RLU).

Figure S6. Changes in cell-associated viral DNA in mononuclear cells isolated from tissue compartments in RMs treated with TLR7 agonist. Proviral DNA (copies/10^6 CD4+ memory cells) was assessed at pre- and post-TLR7 agonist treatment in tissues. Each panel represents proviral DNA measured in peripheral blood mononuclear cells (PBMC), lymph node mononuclear cells (LNMC), and gut mucosa mononuclear cells (GMMC) in RMs. Changes in SIV DNA between pre- and post-treatment was compared using a Wilcoxon matched paired test.

Figure S7. The kinetics of SIV plasma RNA rebound after ART cessation. SIV rebound kinetics following ART cessation was assessed (**A**). Median value of $\log_{10}$ SIV RNA copies/mL for each RM in both GS-986 treated (●, n=4) and control (●, n=6) groups with nine additional control RMs (○) is shown relative to the day of ART stop (Day 0). One animal from control group with low viremia was indicated as an outlier ( ). Log plasma virus RNA was assessed in SIV-infected RMs between days 1 to 56 following ART stop (**B**). Compasiron of TLR7 and control group from study 1 and with additional nine control RMs (**C**) is shown. The plasma SIV RNA was assessed between days 14-21 (Week 2-3) and 49-56 (Week 7-8) following ART cessation, representing peak and set-point viral load, respectively. Area under the curve calculations for the plasma SIV RNA burden were assessed though days 56 post ATI. The results are expressed as the median with interquartile range. The comparison between groups was determined using a Mann-Whitney test.

Figure S8A. Potent activation of CD16+ and CD16-CD56- NK cell subsets by TLR agonist exposure. Activation of $CD16^+$, $CD16^-CD56^+$, and $CD16^-CD56^-$ NK cells in the peripheral blood of vehicle (—), GS-986, 0.01 mg/kg (—), GS-9620, 0.05 mg/kg (—), and GS-9620, 0.15 mg/kg (—) treated monkeys was monitored by flow cytometric detection of CD69. CD69 expression within each subset was measured at time of dose and at 24, 48, and 72 (doses 1-7 only) hours post-dose (time points indicated by x-axis ticks) for doses 1, 3, 5, and 7 (**left**) and doses 11-19 (**right**). Shown are the differences in percent $CD69^+$ cells compared to day of dose.

Figure S8B. Modulation of B cells by TLR agonists. Activation of naïve ($CD27^-$) and memory ($CD27^+$) B cells in the peripheral blood of vehicle (—), GS-986, 0.01 mg/kg (—), GS-9620, 0.05 mg/kg (—), and GS-9620, 0.15 mg/kg (—) treated monkeys was monitored by flow cytometric detection of CD38. CD38 geometric mean fluorescence (GMF) expression within each subset was measured at time of dose and at 24, 48, and 72 (doses 1-7 only) hours post dose (time points indicated by x-axis ticks) for doses 1, 3, 5, and 7 (**left**) and doses 11-19 (**right**). Shown are the differences in normalized CD38 GMF compared to day of dose.

Figure S9. Magnitude of viral reactivation following repeated TLR7 agonist exposure. The AUC of SIV plasma RNA copies was used as a measure of the total amount of SIV reactivation occurring in RMs during 0-72 h post each TLR7 agonist dose. **A.** RMs were treated with escalating doses of GS-986. **B.** Groups of RMs treated with vehicle (control), 0.1 mg/kg GS-986, 0.05 mg/kg or 0.15 mg/kg of GS-9620 are shown. Line and error bars represent the mean and standard deviation (SD).

Figure S10. Induction of ISGs by TLR7 agonist dosing. Heatmap depiction of gene expression patterns of ISG-15, Mx-1 and OAS-1 in RMs from vehicle (n=2), GS-986, 0.1mg/kg (n=3), GS-9620, 0.05mg/kg (n=3) and GS-9620, 0.15mg/kg (n=3) groups. Values reflect fold changes of

mRNA expression of three ISGs at 24, 48, and 72 hours after each TLR7 agonist dose compared to that of baseline are shown by group and number of TLR7 doses.

Figure S11. Changes in cytokines and chemokines after TLR7 agonist administration.

Changes in the level of various inflammatory cytokines and chemokines were measured in plasma between pre- and 24 hours after each TLR7 agonist dose. Values reflecting fold changes of the amounts of inflammatory cytokines and chemokines detected in plasma isolated from four monkeys treated with escalating doses of TLR7 agonist (GS-986) **(A)** and the association of TLR7 doses with cytokine/chemokine induction was assessed in groups of monkeys treated with escalating doses of GS-986 or vehicle (control) (**B**). Fold changes in the amounts of cytokines and chemokines indicated in groups of monkeys treated with vehicle (control), GS-986 (0.1 mg/kg) and GS-9620 (0.05 mg/kg, 0.15 mg/kg) compared to baseline are shown (**C**). Association of TLR7 agonist doses and the amount of cytokine and chemokine induced is shown (**D**). Values are expressed as mean ± standard deviation (SD). Validated ELISA assays were used to determine concentration of cytokines and chemokines including IL-1RA, IL-6, TNF-α, GM-CSF, TGF-β, IL-8, I-TAC, MCP-1, RANTES, and sCD40L as described in Methods. Association of TLR7 dose responses with cytokine/chemokine induction was assessed in groups of monkeys treated with escalating doses of GS-986 (**C, Study 1**), or 0.1 mg/kg of GS-986, 0.05 mg/kg or 0.15 mg/kg of GS9620 (**D, Study 2**). Volcano plots show up/down regulation of cytokine and chemokine levels as response to TLR7 agonist dose. The relative ratio of cytokine and chemokines levels after TLR7 dose was compared to that of the base line. Values that showed statistically significant changes from baseline are shown in red.

Figure S12. Anamnestic SIV Gag-specific CD4+ and CD8+ T cell responses following study 2 ART stop. Shown are the frequencies of IFN-γ-producing SIV Gag-specific CD4+ and CD8+ T cells, measured by intracellular cytokine staining, on the day of ART stop (day 0) and on days 35

and 177 after stop. The background-subtracted percent of IFN-γ-positive CD4+ T (left panel) and CD8+ T (right panel) are shown for monkeys that became viremic (closed symbols) or remained aviremic (open symbols) in each treatment group.

Figure S13 Co-culture of CEMx174 cells with PBMC after ART stop. PBMC were isolated from two control RMs (162-09 and 305-10) and two aviremic RMs (177-10 and 344-10) on days 182 post ATI and used in viral outgrowth assay (**A**) and *in vitro* co-culture assay with susceptible CEMx174 cells following CD8+ T cell depletion (**B**).

Figure S14. ***In vivo*** **CD8+ lymphocyte depletion**. CD8+ lymphocytes were depleted *in vivo* using monoclonal antibody MT807R1 in two viremic animals (288-10 and 295-10) and the two aviremic RMs (177-10 and 344-10). The presence of CD8+ lymphocytes in the peripheral blood was monitored by flow cytometry. The plots of CD8 and CD3 fluorescent antibody staining up to day 35 post depletion are shown.

Figure S15. Viral dynamics modeling of viral blips, rebound, and control. Schematic of the viral dynamics model used to describe i) viral decay after ART initiation, ii) viral production from latently infected cells during TLR7-agonist administration, and iii) viral rebound following ART cessation (**A**). We assume ART inhibits viral infectivity, and TLR7-agonist transiently stimulates reactivation of latent cells. Summary of the differences in rebound kinetics between treated and control animals (**B**). Each curve is generated using the geometric mean of the parameter values from each group. Values of viral dynamics parameters during rebound estimated from model fits (**C - F**). Control and treatment animals from both study phases were pooled for comparisons between groups. Statistical tests took into account the uncertainty in parameter estimates from each animal. The distribution of rebound times was predicted as a function of the reduction in the reservoir size, using a separate stochastic model of viral

reactivation and rebound (**G**). Survival curves show the predicted percentage of animals that have not yet rebounded as a function of time after ART cessation. The median posterior probability (and 95% credible interval) for the reservoir reduction caused by treatment, as a function of the current time off ART without rebound (**H**). We assume a baseline reservoir size of ~ 1 IUPM. At the time of ART interruption, a negative viral outgrowth assay suggests that the reservoir is decreased by 0.8 [0.15-1.95] log. After 6 months without rebound, the updated estimate for the reservoir reduction is 2.6 [1.5-4.0] logs, and after 2 years the estimate is 3.15 [2.05-4.5] logs (or 1,400 [110-32,000]–fold decrease). Details of all the modeling are described in the Supplementary Methods.

Figure S16. Individual fits of viral dynamics model to viral load data. Time course of observed viral dynamics (black dots) and model fits (solid lines) for control (red) and treated (blue) animals. Viral load is shown from the time ART is initiated until the end of the study period. Dots are shown at each time point at which viral load was measured. Model fits were generated using the maximum likelihood estimate for each parameter value. Separate models were used to fit the time from ART initiation to undetectable viremia, viral blips, and viral rebound (see Supplementary Methods for details).

Supplementary References

1. M.A. Nowak, R.M.C. May. *Virus dynamics: mathematical principles of immunology and virology* (Oxford University Press, USA, 2000).

2. R. Luo R, M.J. Piovoso, J. Martinez-Picado, R. Zurakowski. HIV Model Parameter Estimates from Interruption Trial Data including Drug Efficacy and Reservoir Dynamics. *PLoS ONE*. **7**, e40198. doi:10.1371/journal.pone.0040198 (2012).

3. A.L. Hill, D.I.S. Rosenbloom, F. Fu, M.A. Nowak, R.F. Siliciano. Predicting the outcomes of treatment to eradicate the latent reservoir for HIV-1. *Proc Natl Acad Sci.* **111,** 13475–13480. doi:10.1073/pnas.1406663111 (2014).

4. L. Rong, A.S. Perelson. Modeling HIV persistence, the latent reservoir, and viral blips. J *Theor Biol*. doi:10.1016/j.jtbi.2009.06.011 (2009).

5. A. Sedaghat, R. Siliciano, C. Wilke. Low-level HIV-1 replication and the dynamics of the resting CD4+ T cell reservoir for HIV-1 in the setting of HAART. *BMC Infect Dis*. **8**, 2. doi:10.1186/1471-2334-8-2 (2008).

6. H.Y. Chen, M.D. Mascio, A.S. Perelson, D.D. Ho, L. Zhang. Determination of virus burst size in vivo using a single-cycle SIV in rhesus macaques. *Proc Natl Acad Sci.* **104**, 19079–19084. doi:10.1073/pnas.0707449104 (2007).

7. R.J. De Boer, R.M. Ribeiro, A.S. Perelson. Current Estimates for HIV-1 Production Imply Rapid Viral Clearance in Lymphoid Tissues. *PLoS Comput Biol.* **6**, e1000906. doi:10.1371/journal.pcbi.1000906 (2010).

8. B. Ramratnam, S. Bonhoeffer, J. Binley, A. Hurley, L. Zhang, *et al*. Rapid production and clearance of HIV-1 and hepatitis C virus assessed by large volume plasma apheresis. *The Lancet.* **354**, 1782–1785. doi:10.1016/S0140-6736(99)02035-8 (1999).

9. F.E. Satterthwaite. An Approximate Distribution of Estimates of Variance Components. *Biom Bull*. **2**, 110–114. doi:10.2307/3002019 (1946).

10. H. Y-C, L. Shan L, N.N. Hosmane, J. Wang, S.B. Laskey, *et al*. Replication-Competent Noninduced Proviruses in the Latent Reservoir Increase Barrier to HIV-1 Cure. *Cell.* **155,** 540–551. doi:10.1016/j.cell.2013.09.020 (2013).

11. K.M. Bruner, N.N. Hosmane, R.F. Siliciano. Towards an HIV-1 cure: measuring the latent reservoir. *Trends Microbiol.* **23**: 192–203. doi:10.1016/j.tim.2015.01.013 (2015).

12. J.B. Whitney, A.L. Hill, S. Sanisetty, P. Penaloza-MacMaster, J. Liu, *et al.* Rapid seeding of the viral reservoir prior to SIV viraemia in rhesus monkeys. *Nature.* **512**, 74–77. doi:10.1038/nature13594 (2014).

13. A.L. Hill, D.I.S. Rosenbloom, J.D. Siliciano, R.F. Siliciano. Insufficient Evidence for Rare Activation of Latent HIV in the Absence of Reservoir-Reducing Interventions. *PLOS Pathog.* **12**, e1005679. doi:10.1371/journal.ppat.1005679 (2016).

14. A.L. Hill, D.I.S. Rosenbloom, E. Goldstein, E. Hanhauser, D.R. Kuritzkes, *et al.* Real-Time Predictions of Reservoir Size and Rebound Time during Antiretroviral Therapy Interruption Trials for HIV. *PLOS Pathog*. **12**, e1005535. doi:10.1371/journal.ppat.1005535 (2016).

15. D.I.S. Rosenbloom, O. Elliott, A.L. Hill, T.J. Henrich, J.M. Siliciano, *et al*. Designing and Interpreting Limiting Dilution Assays: General Principles and Applications to the Latent Reservoir for Human Immunodeficiency Virus-1. *Open Forum Infect Dis.* **2**, ofv123. doi:10.1093/ofid/ofv123 (2015).

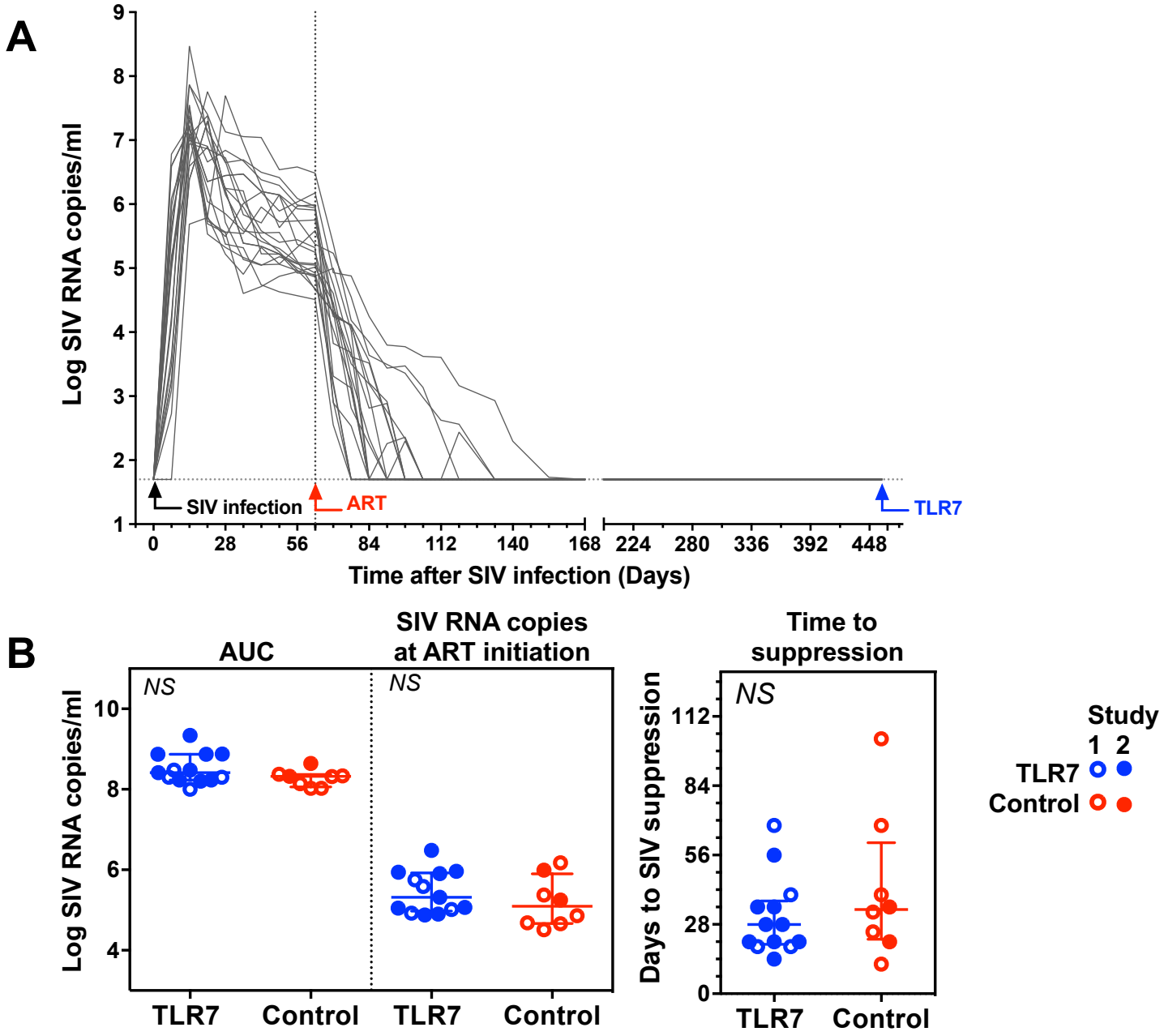
A
Log SIV RNA copies/ml
9
8
7
6
5
4
3
2
1
SIV infection
ART
TLR7
0
28
56
84
112
140
168
224
280
336
392
448
Time after SIV infection (Days)
B
AUC
SIV RNA copies at ART initiation
Time to suppression
NS
NS
NS
Log SIV RNA copies/ml
10
8
6
4
Days to SIV suppression
112
84
56
28
0
TLR7
Control
TLR7
Control
TLR7
Control
Study
1 2
TLR7
Control

Figure S1

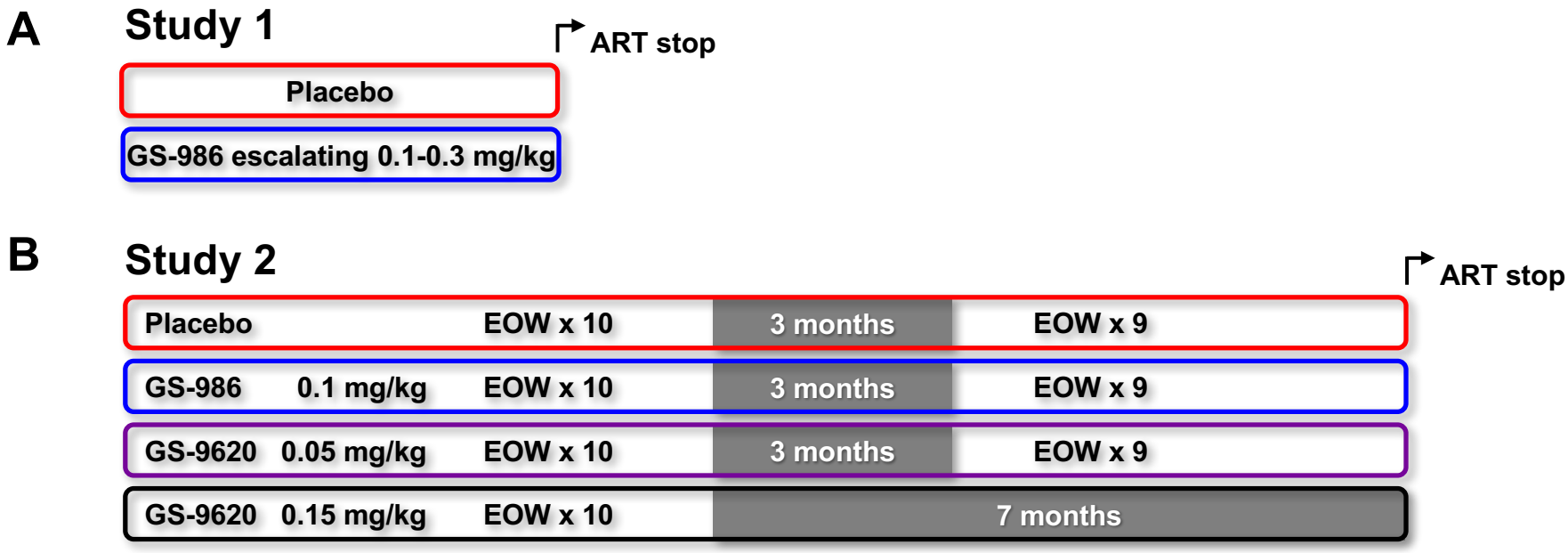
A
Study 1
ART stop
Placebo
GS-986 escalating 0.1-0.3 mg/kg
B
Study 2
ART stop
Placebo
EOW x 10
3 months
EOW x 9
GS-986
0.1 mg/kg
EOW x 10
3 months
EOW x 9
GS-9620
0.05 mg/kg
EOW x 10
3 months
EOW x 9
GS-9620
0.15 mg/kg
EOW x 10
7 months

Figure S2

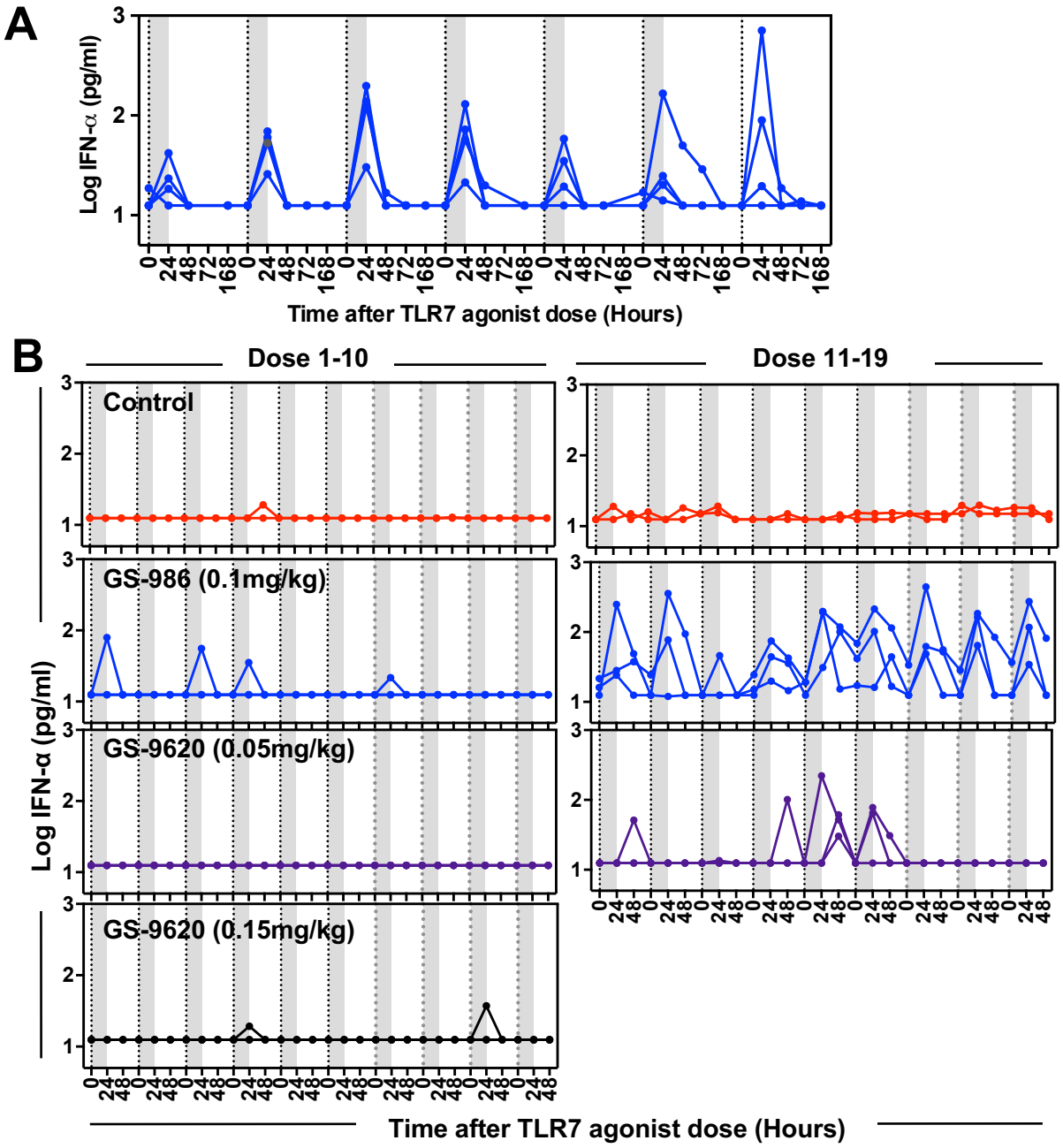
A
Log IFN-α (pg/ml)
Time after TLR7 agonist dose (Hours)
B
Dose 1-10
Dose 11-19
Control
GS-986 (0.1mg/kg)
GS-9620 (0.05mg/kg)
GS-9620 (0.15mg/kg)
Log IFN-α (pg/ml)
Time after TLR7 agonist dose (Hours)

Figure S3

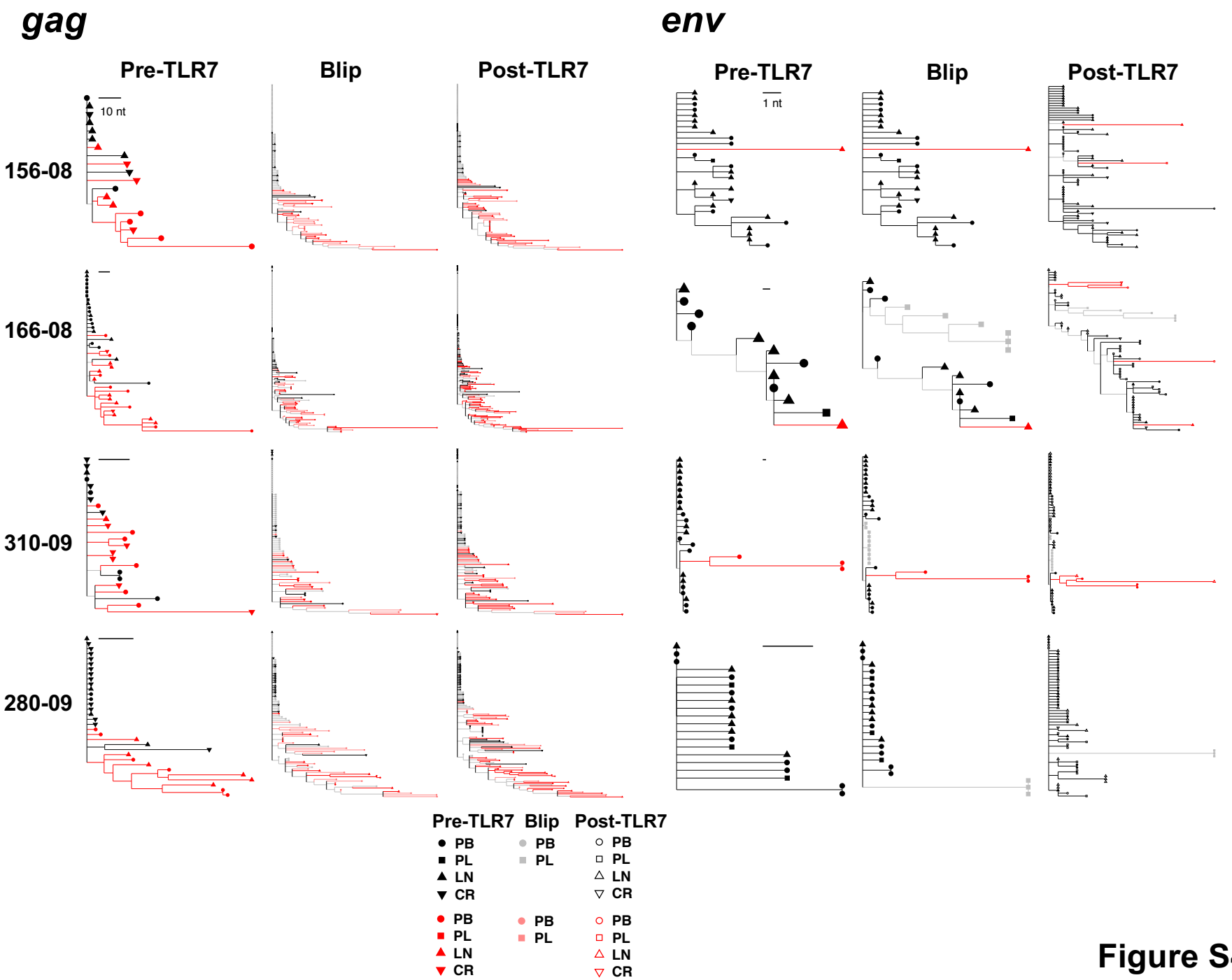
gag
env
Pre-TLR7
Blip
Post-TLR7
Pre-TLR7
Blip
Post-TLR7
10 nt
1 nt
156-08
166-08
310-09
280-09
Pre-TLR7
PB
PL
LN
CR
PB
PL
LN
CR
Blip
PB
PL
PB
PL
Post-TLR7
PB
PL
LN
CR
PB
PL
LN
CR

Figure S4A

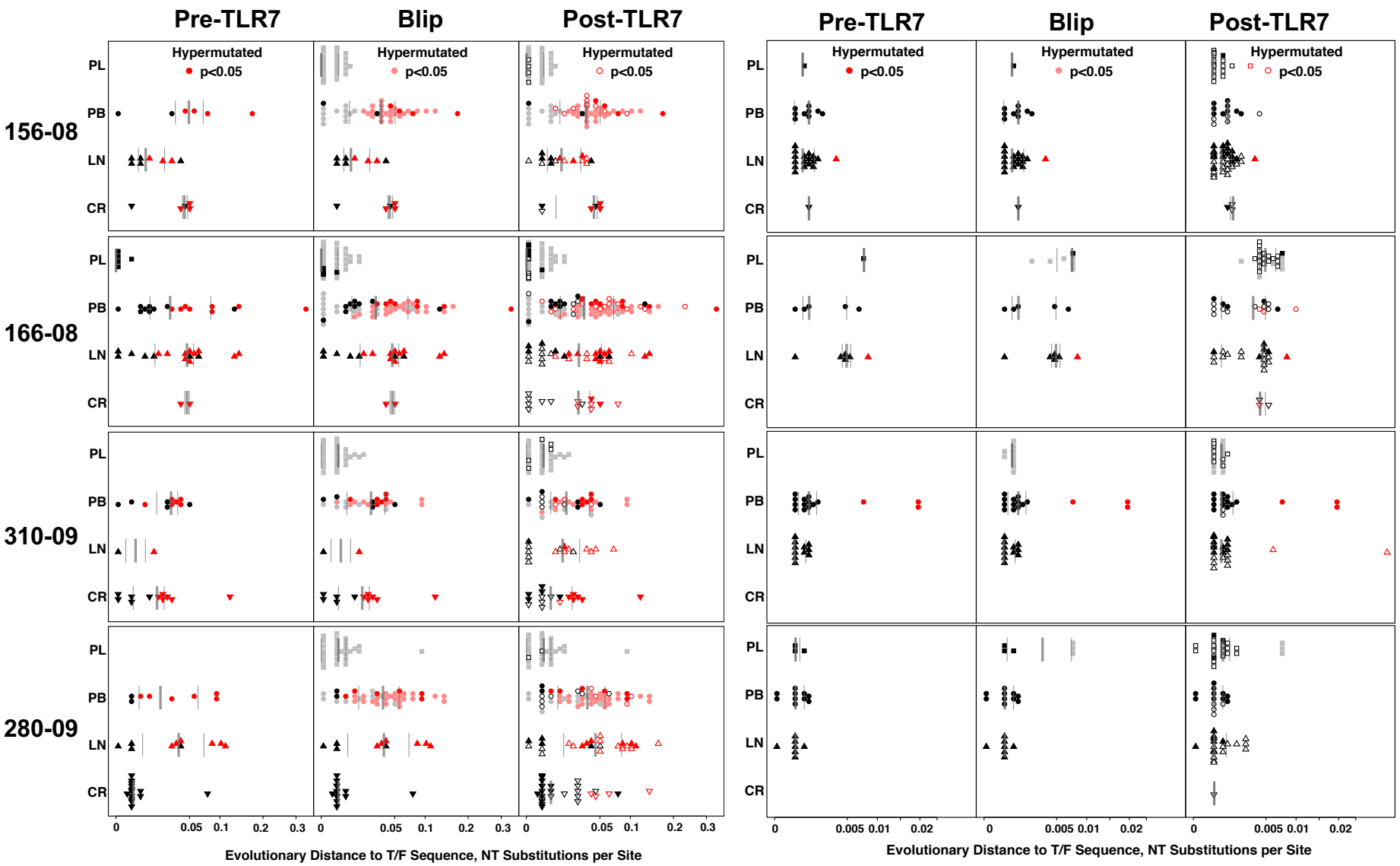
gag
env
Pre-TLR7
Blip
Post-TLR7
Hypermutated
p<0.05
156-08
166-08
310-09
280-09
PL
PB
LN
CR
0
0.05
0.1
0.2
0.3
0.005
0.01
0.02
Evolutionary Distance to T/F Sequence, NT Substitutions per Site

Figure S4B

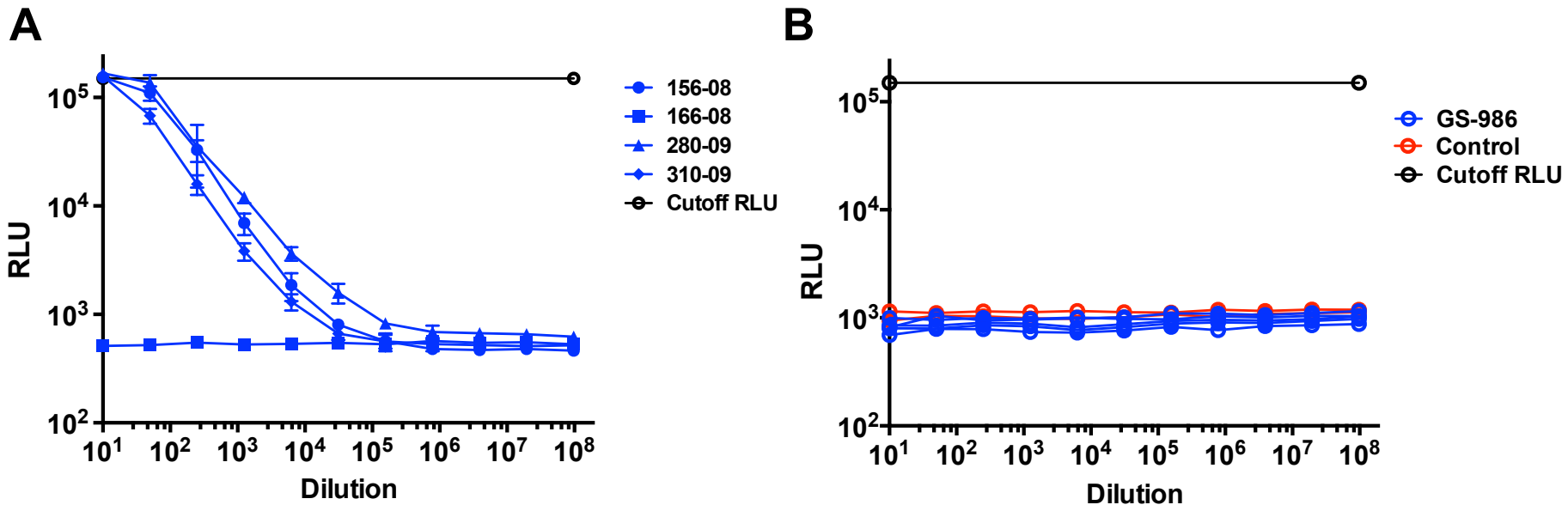
A
RLU
10^5
10^4
10^3
10^2
10^1 10^2 10^3 10^4 10^5 10^6 10^7 10^8
Dilution
156-08
166-08
280-09
310-09
Cutoff RLU
B
RLU
10^5
10^4
10^3
10^2
10^1 10^2 10^3 10^4 10^5 10^6 10^7 10^8
Dilution
GS-986
Control
Cutoff RLU

Figure S5

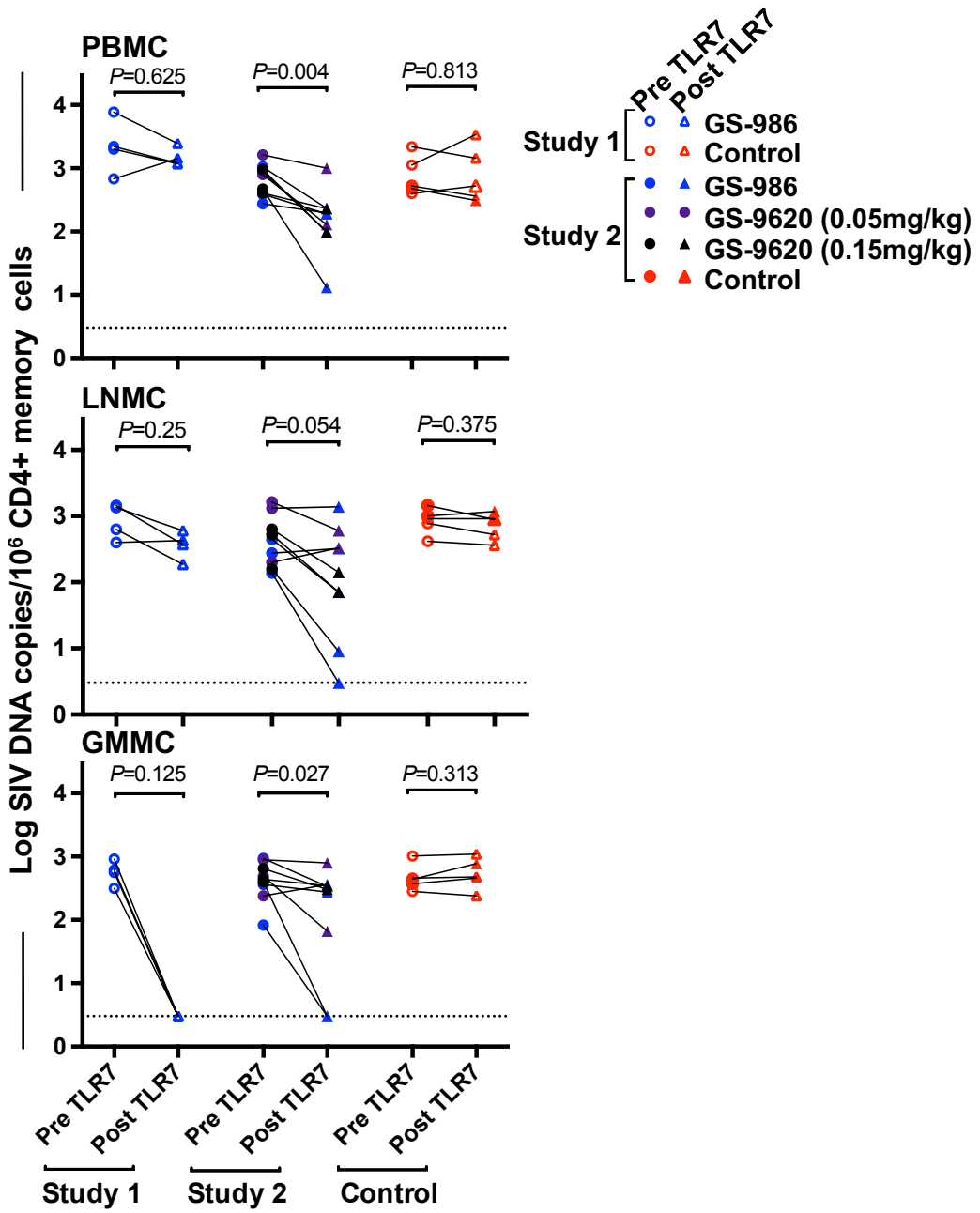
PBMC
LNMC
GMMC
P=0.625
P=0.004
P=0.813
P=0.25
P=0.054
P=0.375
P=0.125
P=0.027
P=0.313
Log SIV DNA copies/10^6 CD4+ memory cells
0
1
2
3
4
Pre TLR7
Post TLR7
Study 1
Study 2
Control
Study 1
GS-986
Control
Study 2
GS-986
GS-9620 (0.05mg/kg)
GS-9620 (0.15mg/kg)
Control

Figure S6

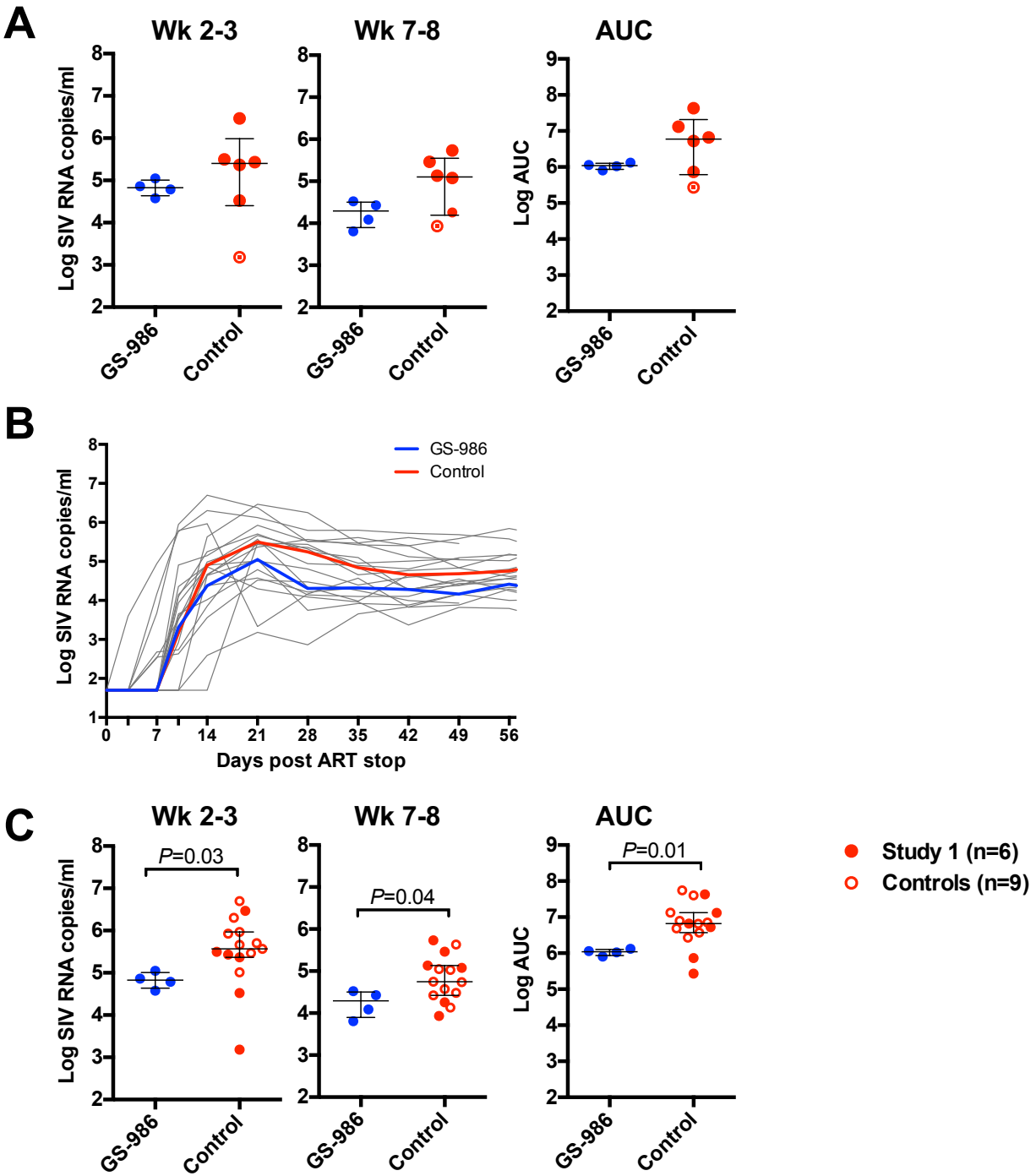
A
Wk 2-3
Wk 7-8
AUC
Log SIV RNA copies/ml
Log AUC
GS-986
Control
B
GS-986
Control
Log SIV RNA copies/ml
Days post ART stop
C
Wk 2-3
Wk 7-8
AUC
P=0.03
P=0.04
P=0.01
Log SIV RNA copies/ml
Log AUC
GS-986
Control
Study 1 (n=6)
Controls (n=9)

Figure S7

A

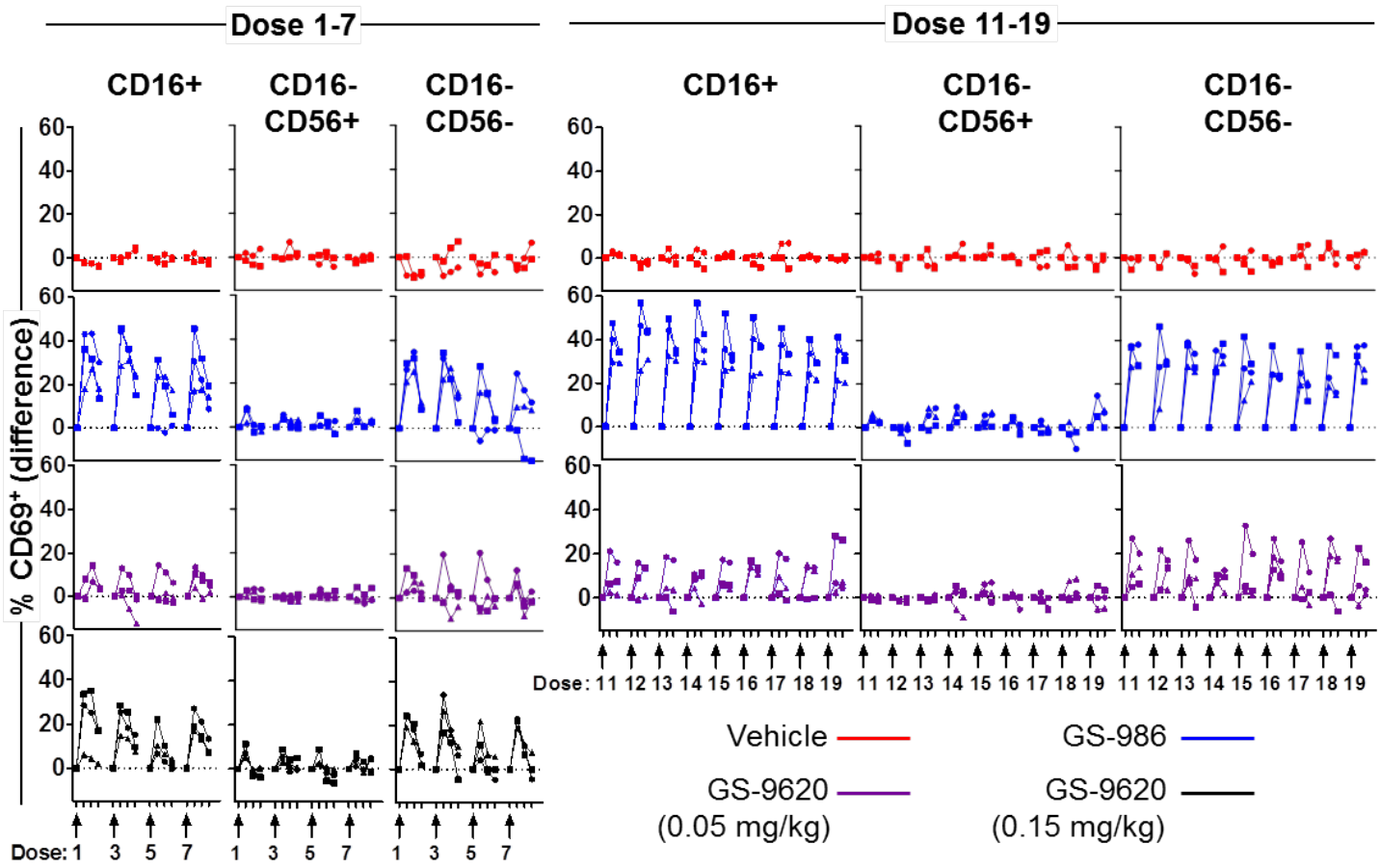
Dose 1-7
Dose 11-19
CD16+
CD16- CD56+
CD16- CD56-
% CD69+ (difference)
60
40
20
0
Dose: 1 3 5 7
Dose: 11 12 13 14 15 16 17 18 19
Vehicle
GS-986
GS-9620 (0.05 mg/kg)
GS-9620 (0.15 mg/kg)

Figure S8A

B

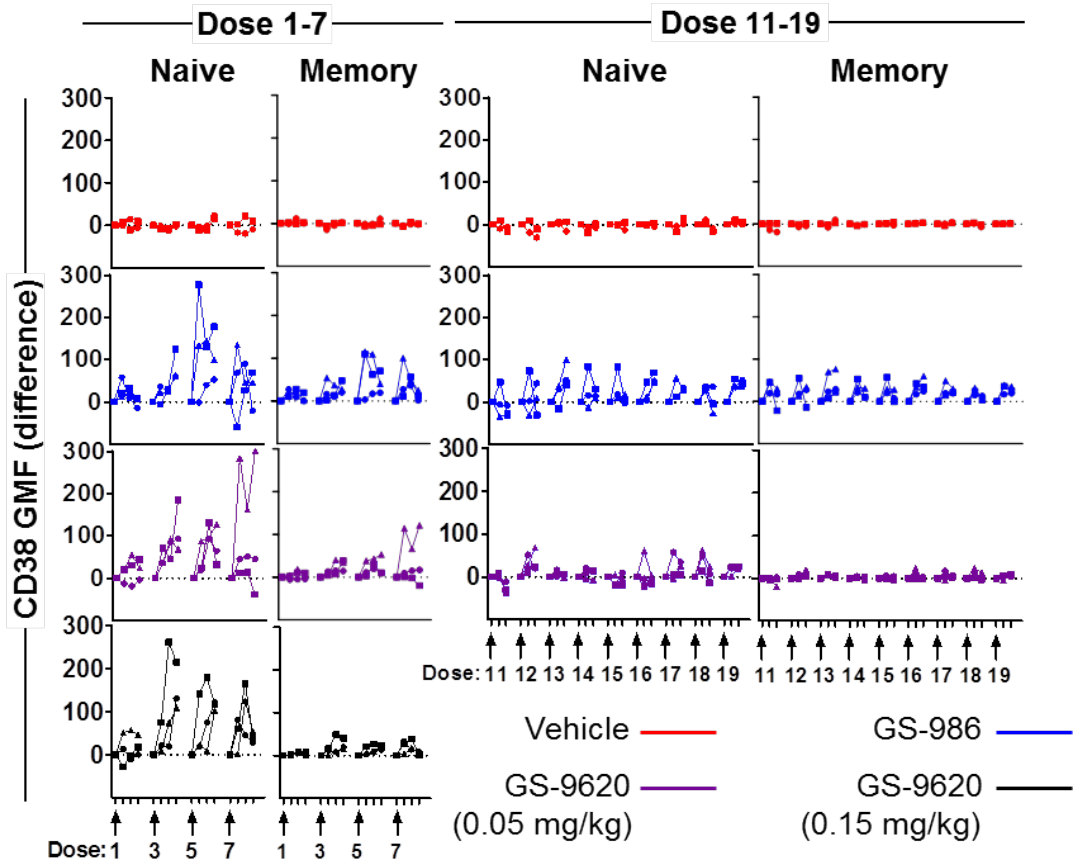
Dose 1-7
Dose 11-19
Naive
Memory
Naive
Memory
CD38 GMF (difference)
300
200
100
0
Dose: 1 3 5 7
1 3 5 7
Dose: 11 12 13 14 15 16 17 18 19
11 12 13 14 15 16 17 18 19
Vehicle
GS-986
GS-9620 (0.05 mg/kg)
GS-9620 (0.15 mg/kg)

Figure S8B

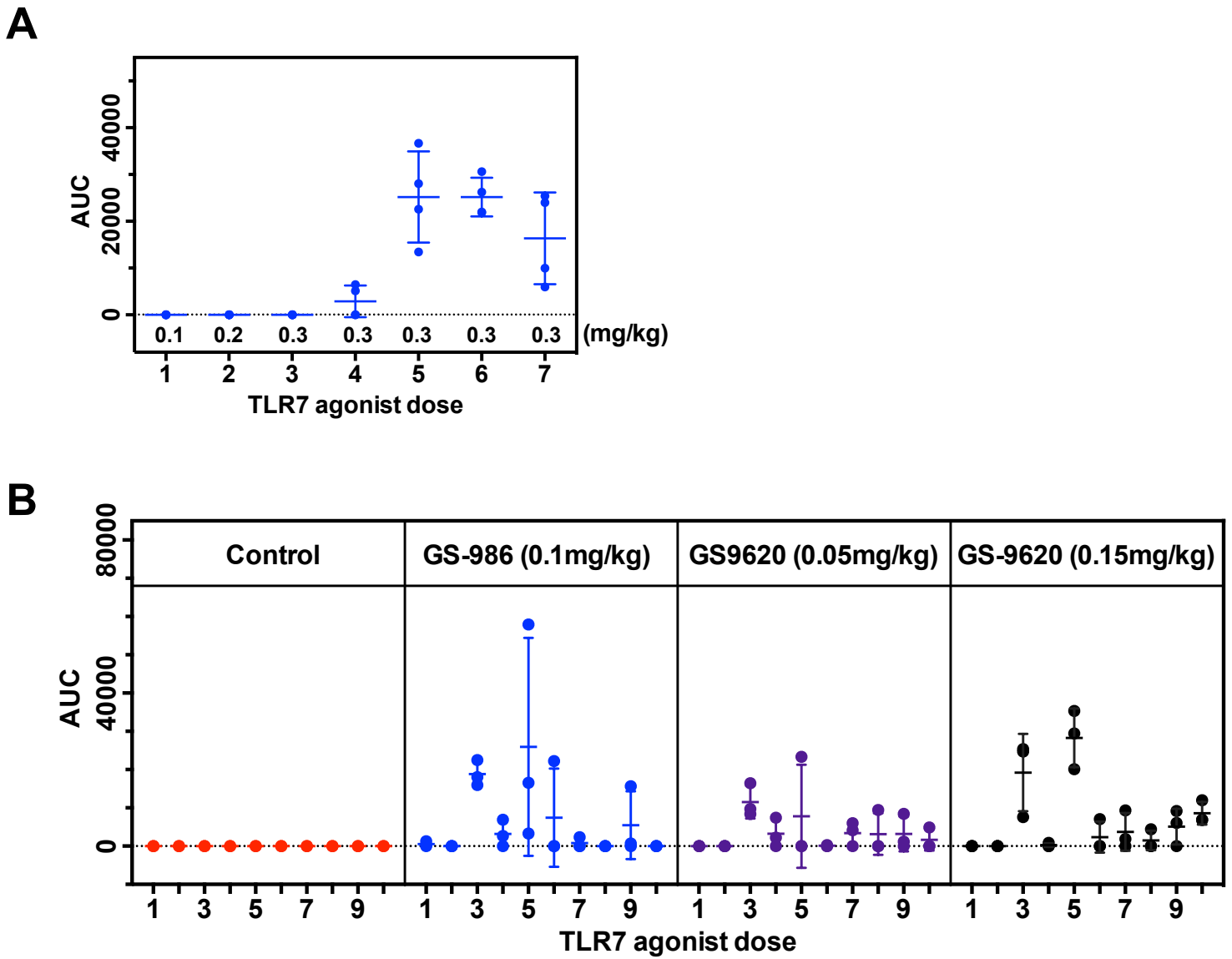
A
AUC
0
20000
40000
0.1
0.2
0.3
0.3
0.3
0.3
0.3
(mg/kg)
1
2
3
4
5
6
7
TLR7 agonist dose
B
Control
GS-986 (0.1mg/kg)
GS9620 (0.05mg/kg)
GS-9620 (0.15mg/kg)
AUC
0
40000
80000
1
3
5
7
9
TLR7 agonist dose

Figure S9

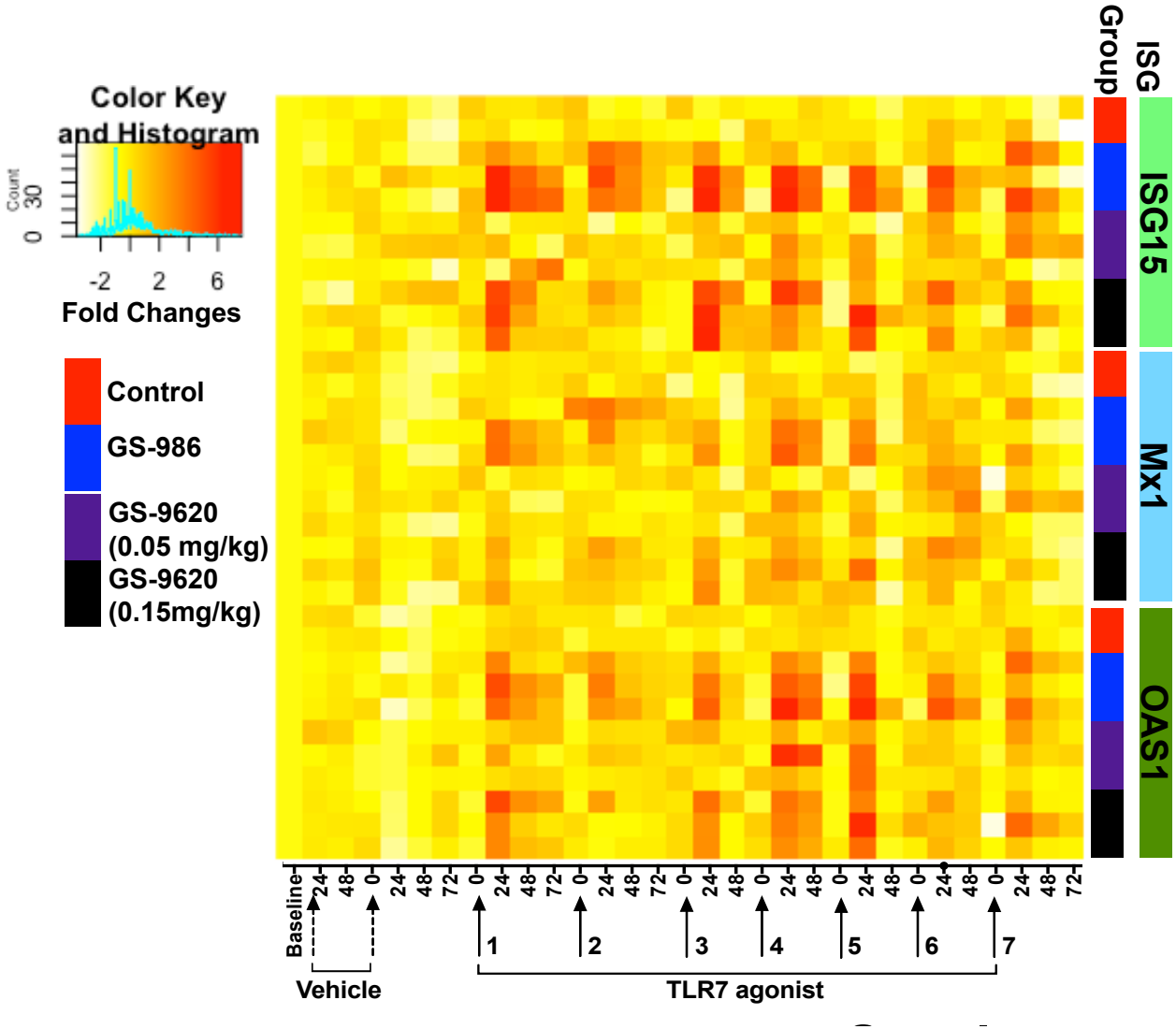
Color Key
and Histogram
Count
0
30
-2
2
6
Fold Changes
Control
GS-986
GS-9620
(0.05 mg/kg)
GS-9620
(0.15mg/kg)
Group
ISG
ISG15
Mx1
OAS1
Baseline
Vehicle
TLR7 agonist
1
2
3
4
5
6
7

Figure S10

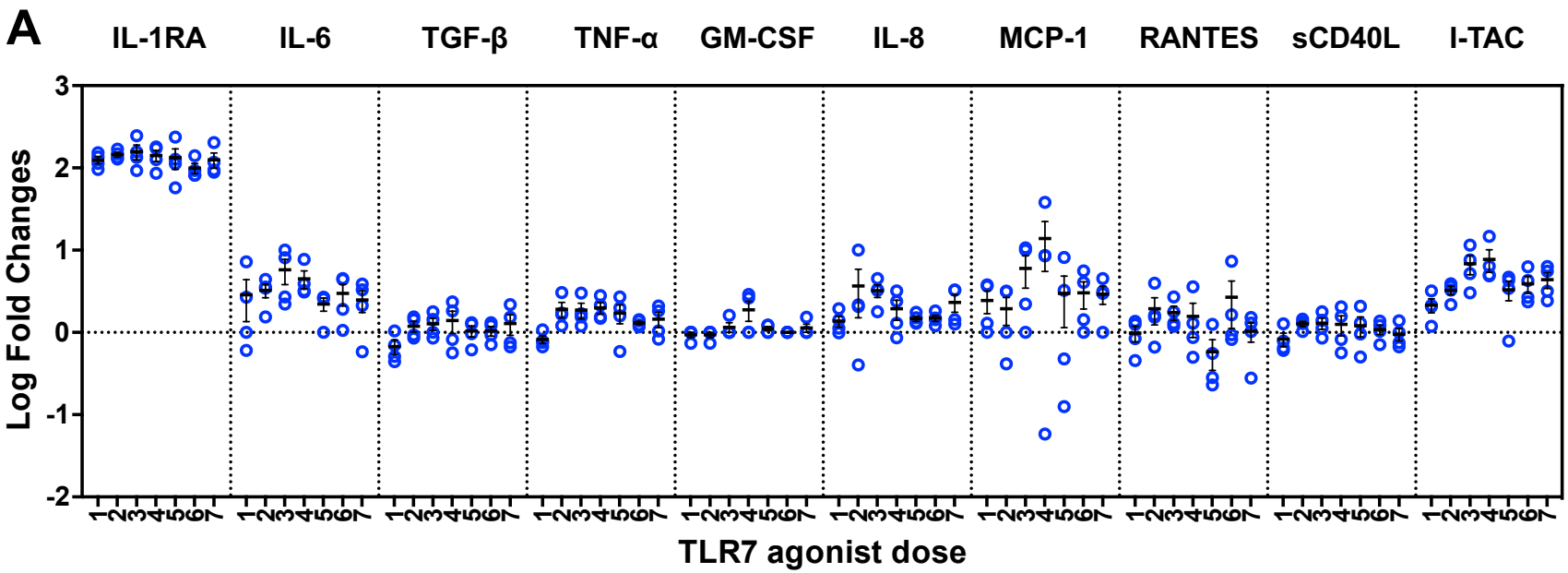

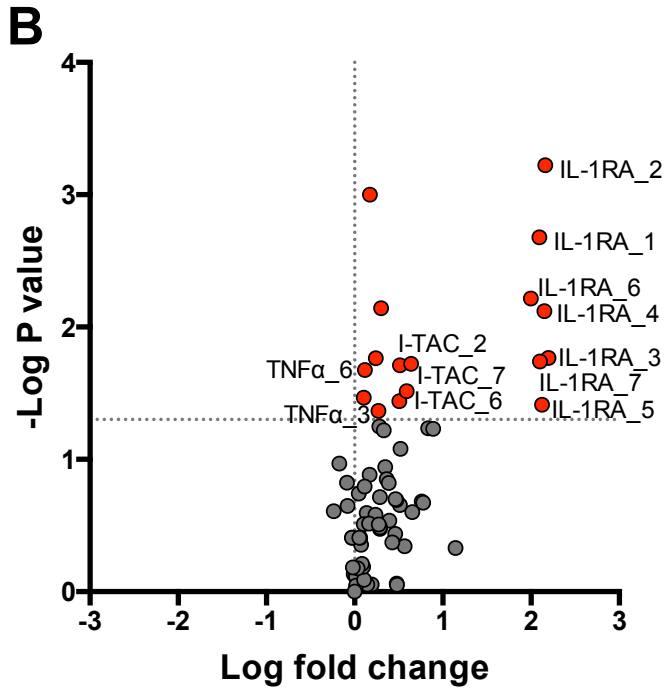

Figure S11AB

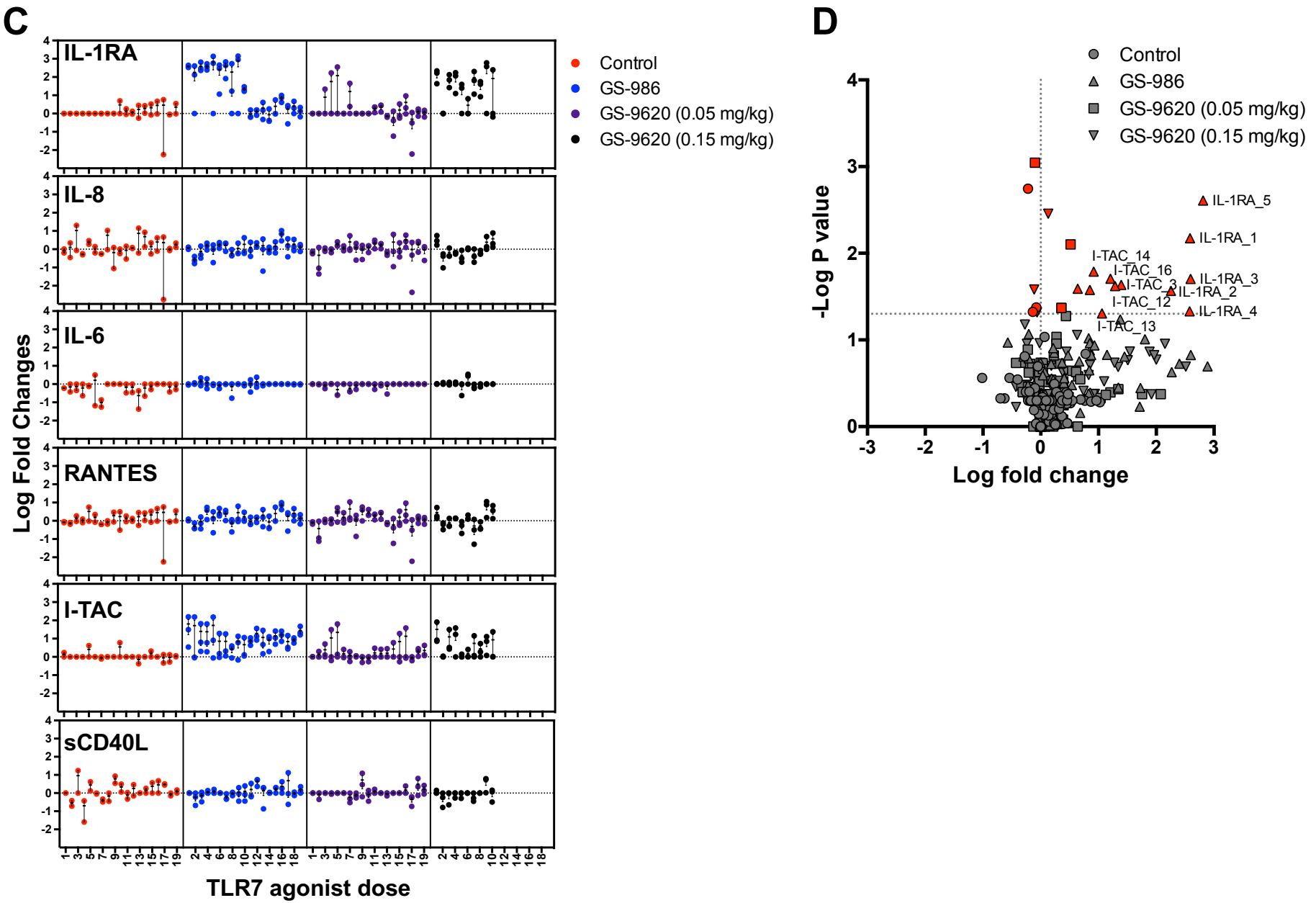

Figure S11CD

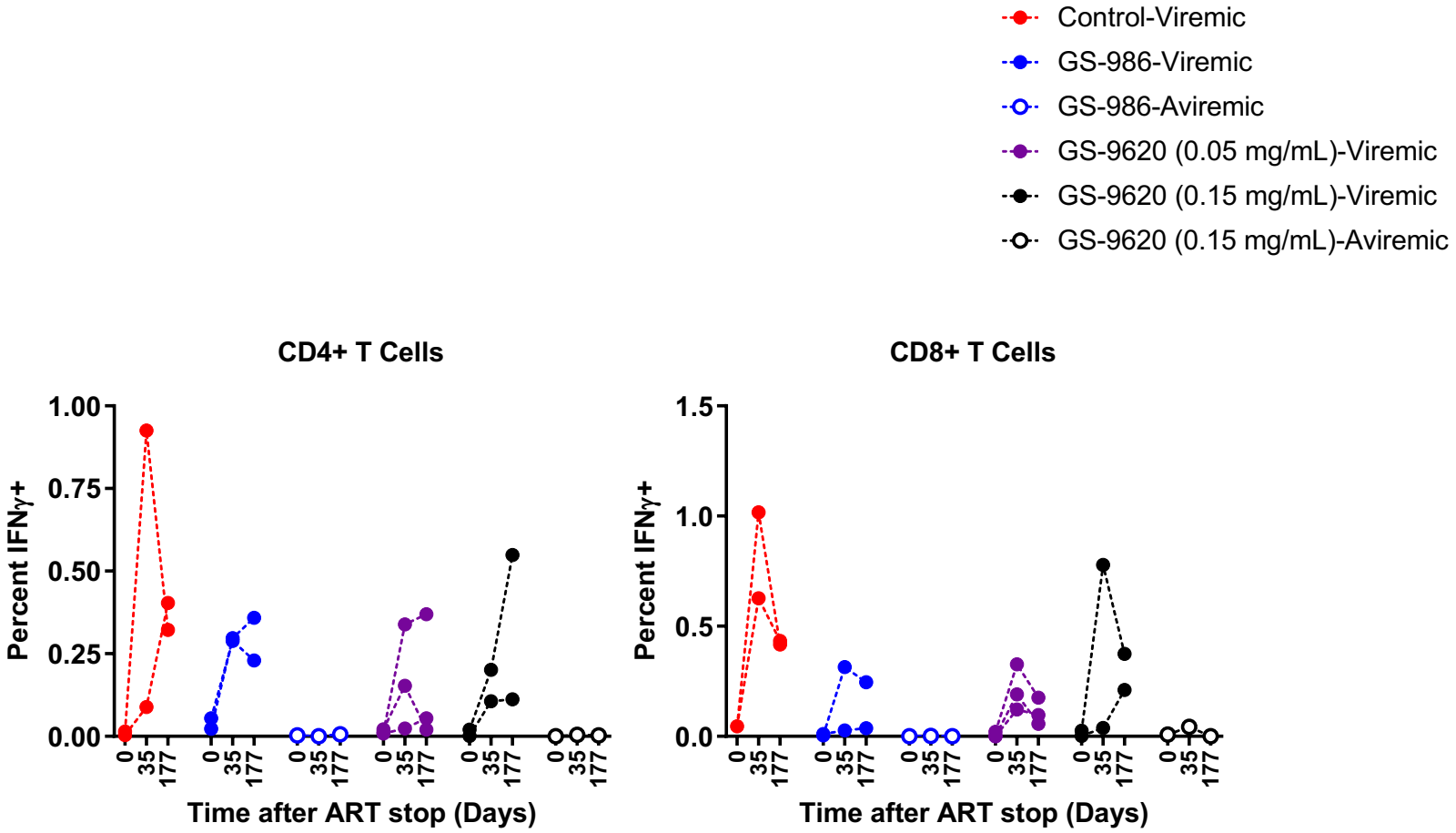
Control-Viremic
GS-986-Viremic
GS-986-Aviremic
GS-9620 (0.05 mg/mL)-Viremic
GS-9620 (0.15 mg/mL)-Viremic
GS-9620 (0.15 mg/mL)-Aviremic
CD4+ T Cells
CD8+ T Cells
Percent IFNγ+
1.00
0.75
0.50
0.25
0.00
1.5
1.0
0.5
0.0
0
35
177
Time after ART stop (Days)

Figure S12

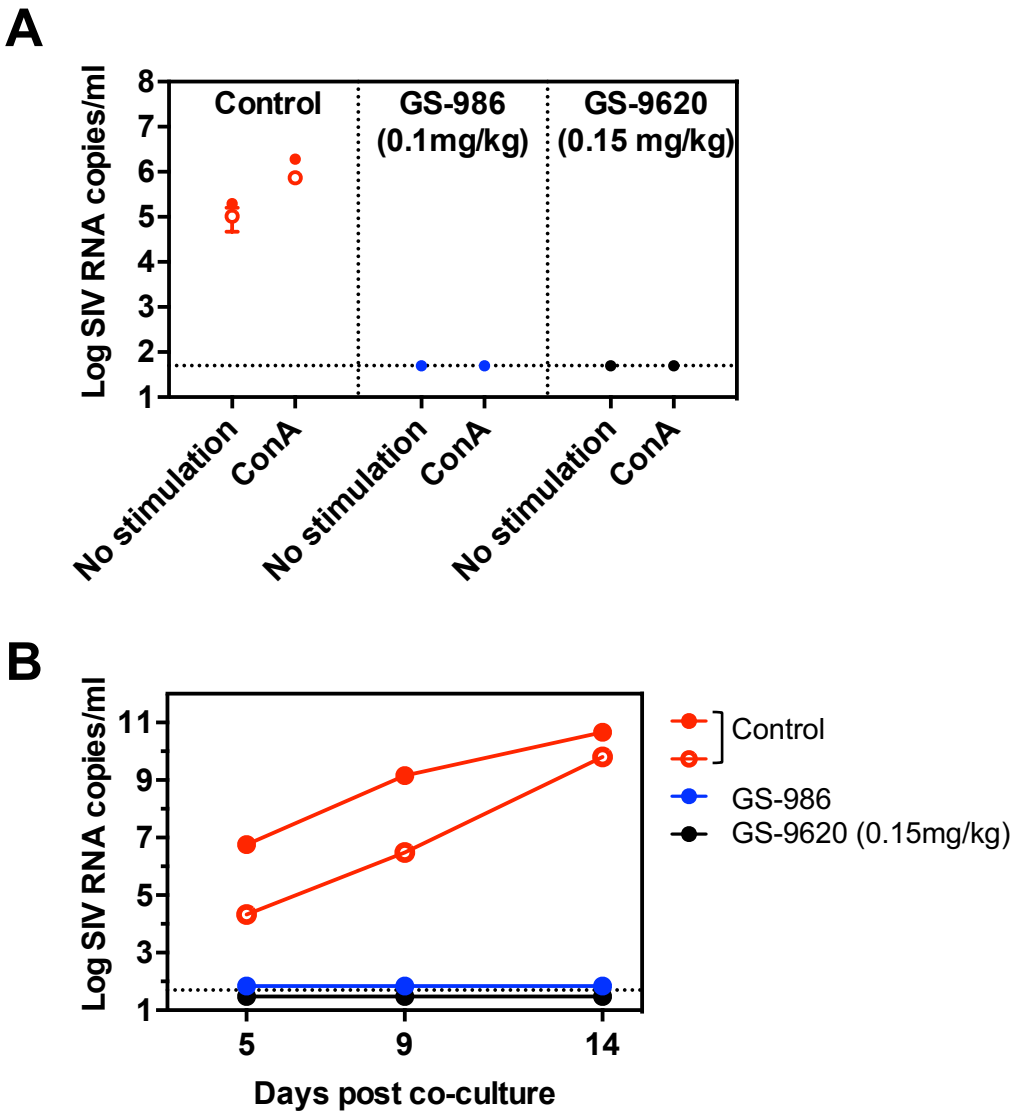
A
Log SIV RNA copies/ml
8
7
6
5
4
3
2
1
Control
GS-986
(0.1mg/kg)
GS-9620
(0.15 mg/kg)
No stimulation
ConA
No stimulation
ConA
No stimulation
ConA
B
Log SIV RNA copies/ml
11
9
7
5
3
1
5
9
14
Days post co-culture
Control
GS-986
GS-9620 (0.15mg/kg)

Figure S13

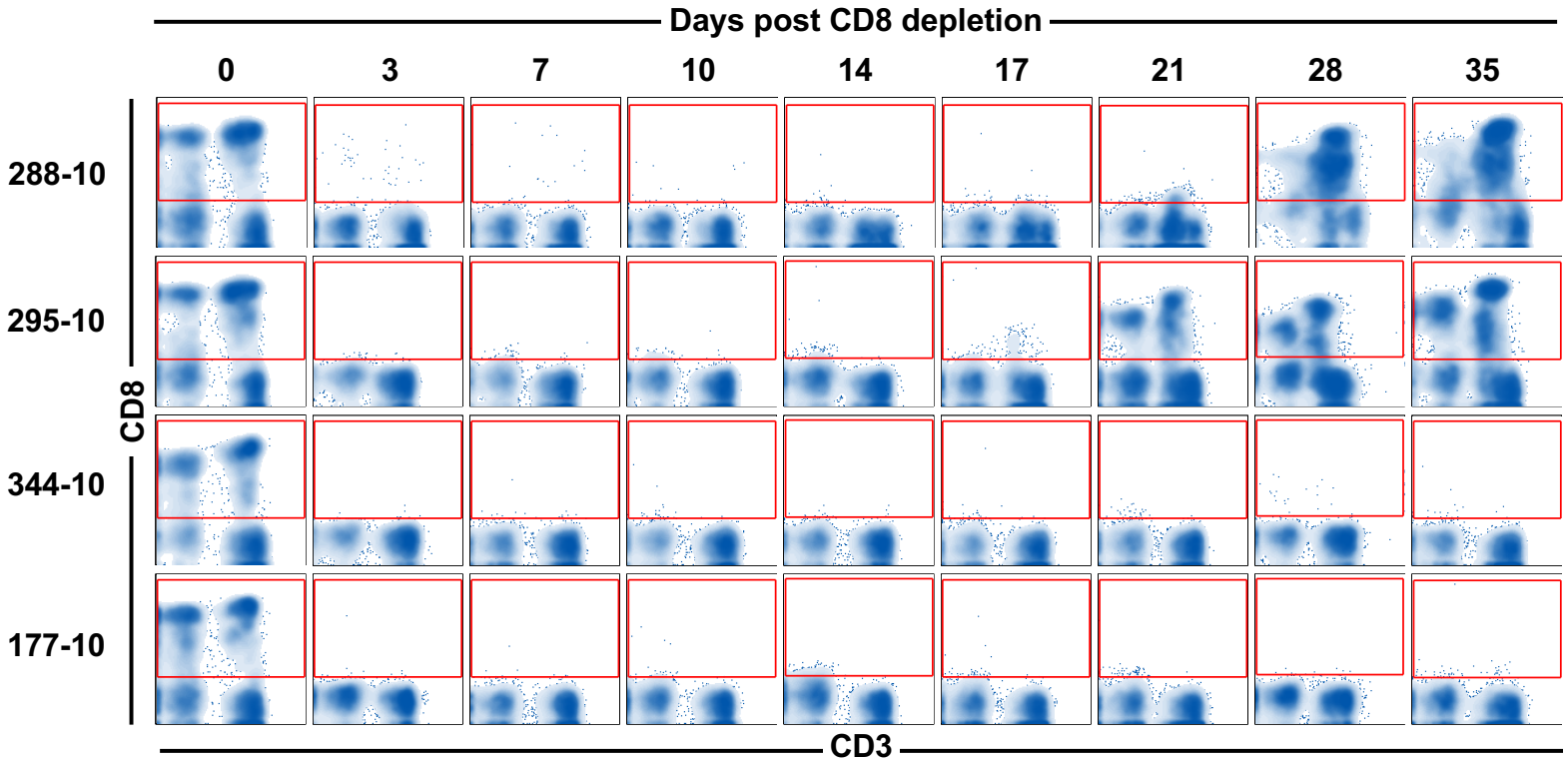
Days post CD8 depletion
0
3
7
10
14
17
21
28
35
288-10
295-10
344-10
177-10
CD8
CD3

Figure S14

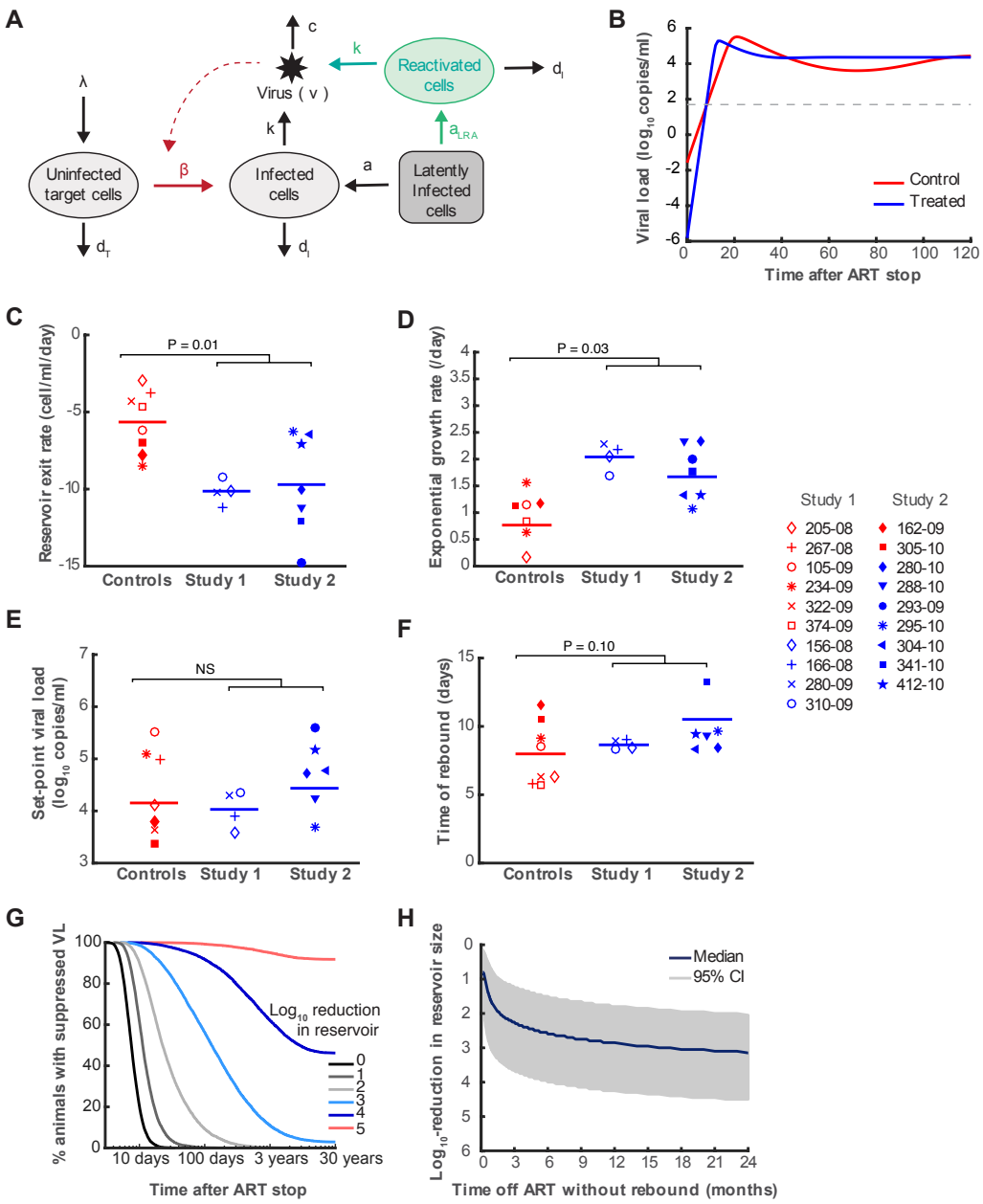
A
c
k
Reactivated cells
d_l
λ
Virus (v)
k
a_{LRA}
Uninfected target cells
β
Infected cells
a
Latently Infected cells
d_T
d_l
B
Viral load (log_{10} copies/ml)
Control
Treated
Time after ART stop
C
Reservoir exit rate (cell/ml/day)
P = 0.01
Controls
Study 1
Study 2
D
Exponential growth rate (/day)
P = 0.03
Controls
Study 1
Study 2
Study 1
Study 2
205-08
267-08
105-09
234-09
322-09
374-09
156-08
166-08
280-09
310-09
162-09
305-10
280-10
288-10
293-09
295-10
304-10
341-10
412-10
E
Set-point viral load (log_{10} copies/ml)
NS
Controls
Study 1
Study 2
F
Time of rebound (days)
P = 0.10
Controls
Study 1
Study 2
G
% animals with suppressed VL
Log_{10} reduction in reservoir
0
1
2
3
4
5
10 days
100 days
3 years
30 years
Time after ART stop
H
Log_{10}-reduction in reservoir size
Median
95% CI
Time off ART without rebound (months)

Figure S15

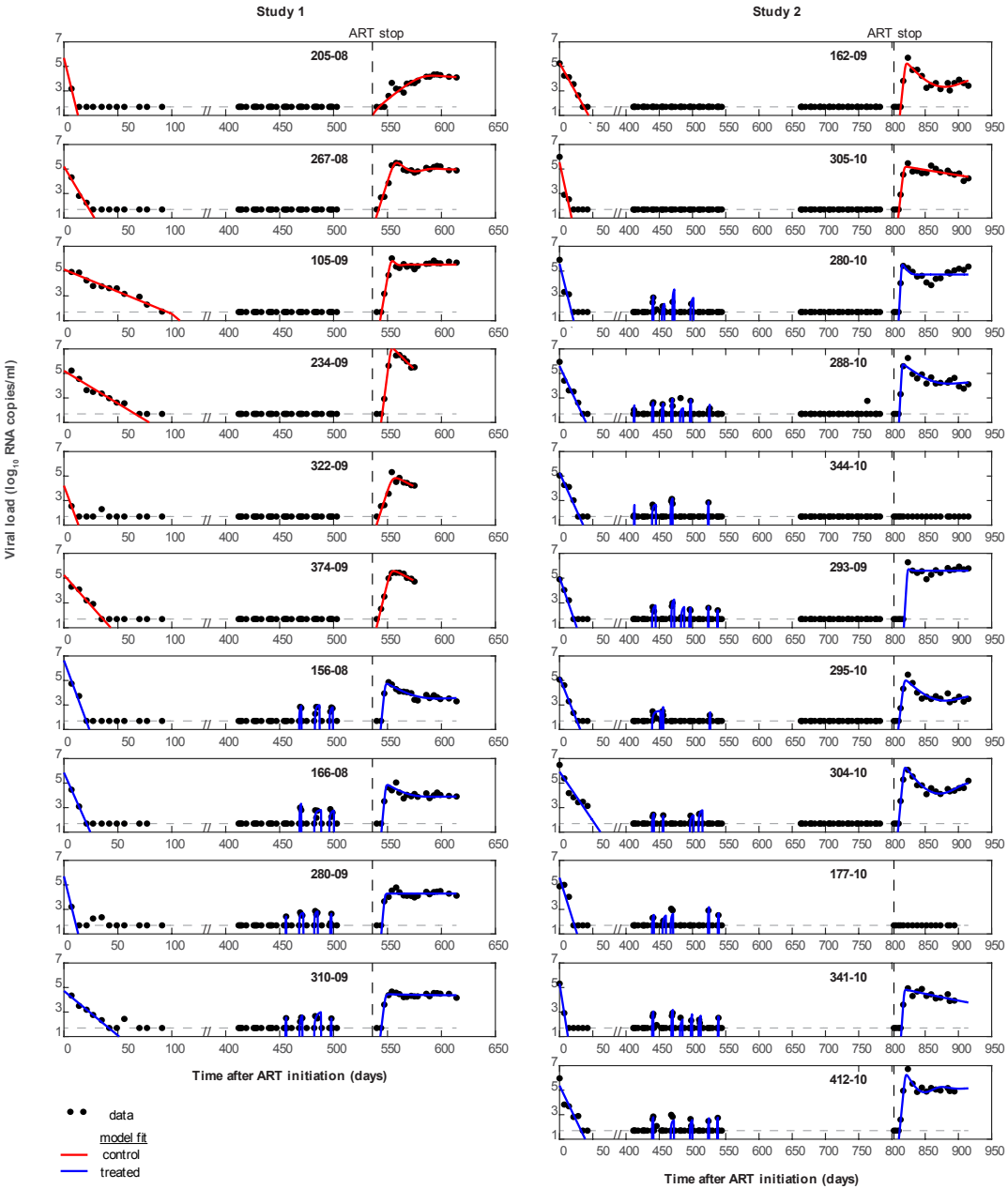
Study 1
Study 2
ART stop
205-08
267-08
105-09
234-09
322-09
374-09
156-08
166-08
280-09
310-09
162-09
305-10
280-10
288-10
344-10
293-09
295-10
304-10
177-10
341-10
412-10
Viral load (log10 RNA copies/ml)
Time after ART initiation (days)
data
model fit
control
treated

Figure S16